

# Picoplanktonic methane production in eutrophic surface waters

Sandy E. Tenorio<sup>1, 2, 4</sup>, Laura Farías<sup>1, 2, 3</sup>

<sup>1</sup>Departamento de Oceanografía, Facultad de Ciencias Naturales y Oceanográficas, Universidad de Concepción, Concepción, 4070043, Chile.

<sup>2</sup>Centro de Ciencia del Clima y la Resiliencia (CR2), Chile.

<sup>3</sup>Instituto Milenio en Socio-ecología Costera (SECOS), Chile.

<sup>4</sup>Programa de Graduados en Oceanografía, Departamento de Oceanografía, Universidad de Concepción, Concepción, 4070043, Chile.

*Correspondence to:* Laura Farías (laura.farias@udec.cl)

**Abstract.** Over the past decade, extensive research has delved into the methane (CH<sub>4</sub>) paradox which involves aerobic CH<sub>4</sub> production. We present noteworthy observations of CH<sub>4</sub> oversaturation within the surface layer of the central Chile upwelling zone (36° S, 73° W) over two consecutive seasonal cycles (2018-2021). Complementing these observations, CH<sub>4</sub> cycling experiments were conducted, utilizing distinct plankton fractions (encompassing the natural planktonic community, fractions <150 μm, <3 μm, and <0.2 μm), in different productivity periods of phytoplanktonic production/composition throughout the year. Our findings underscore the pivotal role of picoplankton (<3 μm) in CH<sub>4</sub> production on the ocean surface, contrasting with the limited contribution of larger microorganisms (<150 μm). Notably, incubations with methylated substrates, such as methylphosphonic acid (MPn) and trimethylamine (TMA), induce heightened CH<sub>4</sub> production within the picoplanktonic fraction. This phenomenon is consistently observed during both upwelling (austral spring-summer) and non-upwelling (winter) seasons, with significance in the latter period, when *Synechococcus sp.* exhibits notably high relative abundance.

Long-term microcosm experiments highlight the crucial roles played by heterotrophic bacteria and cyanobacteria in methylotrophic methanogenesis. This process enhances CH<sub>4</sub> production, facilitated by the recycling of dissolved organic carbon (DOC). Picoplankton emerges as a pivotal factor influencing the recycling of methylated substrates, and it is responsible for maintaining CH<sub>4</sub> supersaturation. These findings provide valuable insights into the biogeochemical processes driving CH<sub>4</sub> dynamics, particularly in highly productive upwelling areas.

**Key words:** dissolved methane, surface methane production, picoplankton, coastal upwelling.

## Key points:

1. Picoplankton plays a crucial role in maintaining CH<sub>4</sub> supersaturation in the surface layer under different oceanographic conditions, influencing its exchange with the atmosphere.
2. Methylated substrates, such as methylphosphonic acid (MPn) and trimethylamine (TMA), notably stimulate CH<sub>4</sub> production through picoplankton-mediated methylotrophic methanogenesis.
3. *Synechococcus sp.*, utilizing the MPn substrate during the non-upwelling season, and picoeukaryotes, utilizing the TMA substrate during the onset of upwelling, could emerge as crucial microorganisms involved in CH<sub>4</sub> generation.

## 38 1. Introduction

39 Methane (CH<sub>4</sub>) is a short-lived yet potent greenhouse gas, exhibiting a significantly higher heat-trapping capacity than CO<sub>2</sub>  
40 over a century. Its importance lies in its substantial influence on global climate dynamics and the necessity for robust mitigation  
41 strategies (IPCC, 2021; Harmsen et al., 2020). The ocean holds considerable amounts of dissolved and hydrate CH<sub>4</sub>, rendering  
42 its thorough study crucial for precise climate change modelling and comprehending its ecological diversification within  
43 oceanic ecosystems (IPCC, 2021; Xu et al., 2022).

44 The distribution of CH<sub>4</sub> is intricately influenced by both complex physical (transport) and biogeochemical (production and  
45 consumption rates) processes (Reeburgh, 2007). In the open ocean, surface waters generally display slight oversaturation,  
46 whereas deeper waters tend toward equilibrium or undersaturation with respect to the atmosphere. However, there is often  
47 CH<sub>4</sub> accumulation within the pycnocline (Lamontagne et al., 1973; Cicerone and Oremland, 1988; Holmes et al., 2000). These  
48 distribution patterns led to the identification of the CH<sub>4</sub> paradox (see review Reeburgh, 2007). Early hypotheses have suggested  
49 various sources for CH<sub>4</sub> oversaturation in the surface layer, including organic matter respiration within anoxic niches of  
50 particulate organic material (Karl and Tilbrook, 1994), within fish (Oremland, 1979), and zooplankton guts (De Angelis and  
51 Lee, 1994). However, these classical methanogenesis pathways remain obscured in the surface and oxic zone of aquatic  
52 systems. Subsequent advancements in this field highlighted biochemical processes, such as methylotrophic methanogenesis,  
53 now understood as the production of CH<sub>4</sub> from methylated compounds under diverse biogeochemical conditions (Karl et al.,  
54 2008; Damm et al., 2010, 2015; Repeta et al., 2016).

55 Methylated compounds are synthesized or degraded by diverse autotrophic and heterotrophic microorganisms, for example,  
56 *Nitrosopumilus maritimus* produces phosphonates like methylphosphonic acid (MPn) (Metcalf et al., 2012), whereas different  
57 species of phytoplankton, in turn, contribute to sulphur derivatives such as methionine (Lenhart et al., 2016),  
58 dimethylsulfoniopropionate (DMSP), dimethyl sulfide (DMS) (Belviso et al., 1990; Stefels and Van Boekel, 1993) and  
59 trimethylamines (TMA) (Sun et al., 2019), serving as potential carbon sources for microorganisms and thereby contributing  
60 to CH<sub>4</sub> generation via methylotrophic methanogenesis. Furthermore, there is a suggestion that photosynthesis plays a role in  
61 direct CH<sub>4</sub> production (Berg et al., 2014; León-Palmero et al., 2020; Klintzsch et al., 2023). Several studies have shown  
62 associations between CH<sub>4</sub> anomalies in surface waters and specific phytoplanktonic groups, such as coccolithophores (Lenhart  
63 et al., 2016) and cyanobacteria (Bižić et al., 2020). Hence, recognizing phytoplankton in various size fractions as direct links  
64 to CH<sub>4</sub> production in diverse marine ecosystems (Bizic, 2021), becomes imperative, especially through pathways involving  
65 demethylation from methylated compounds (Damm et al., 2010; Florez-Leiva et al., 2013; Lenhart et al., 2016; Karl et al.,  
66 2008; Sun et al., 2011; Repeta et al., 2016).

67 Coastal upwellings, due to their high productivity, represent an emblematic site for the study of CH<sub>4</sub> production, but the  
68 proximity to anoxic sediments and prevalent anaerobic methanogenesis in sediments or in the oxygen minimum zones (OMZ)  
69 often obscures the study of CH<sub>4</sub> generation within oxygen-rich surface waters. Indeed, CH<sub>4</sub> profiles predominantly exhibit  
70 significant increases towards anoxic sediments (Fariás et al., 2021; Ma et al., 2020; Kock et al., 2008). Coastal regions serve

71 as intensive CH<sub>4</sub> sources, facilitating lateral transport to open waters (Borges and Abril, 2012; Upstill-goddard and Barnes,  
72 2016) and/or the atmosphere due to vertical advection linked to coastal upwelling (Farías et al., 2021; Kock et al., 2008).  
73 Current global CH<sub>4</sub> balances exhibit high uncertainty (Saunio et al., 2020; Roth et al., 2022; Lu et al., 2021) and considerable  
74 spatial/temporal variability, particularly in coastal environments, where fluxes represent over 40% of total atmospheric fluxes  
75 (Weber et al., 2019; Bange et al., 1994).

76 Given the upwelling systems are expected to integrate all before mentioned mechanisms, investigating CH<sub>4</sub> dynamics becomes  
77 pivotal. Upwelling processes dynamically transport nutrient-rich water onto continental shelves and surface, significantly  
78 enhancing biological productivity to eutrophic levels. This surge in high microbial productivity, biomass, and organic matter  
79 decomposition, establishing these areas as pivotal hubs for carbon cycling, particularly in CH<sub>4</sub> (Capone and Hutchins, 2013).  
80 Indeed, in upwelling systems a large part of the primary production is channelled to dissolved organic carbon (DOC) through  
81 the microbial food web, and a less percentage directly to copepods via the herbivore food chain (Vargas et al., 2007). In  
82 addition, coastal areas receive large amounts of DOC from rivers (Bianchi, 2011), this is also the case of upwelling systems  
83 off central Chile (Vargas et al., 2013). These microbial food web and riverine pathways not only transport and remineralize  
84 nutrients and DOC but also fosters the generation of greenhouse gases like CH<sub>4</sub> (Dinasquet et al., 2018; Sun et al., 2019).

85 Crucially, specific microbial groups such as Pelagibacter, SAR 11, among other, considered key players in DOC recycling,  
86 have been identified as potential contributors to CH<sub>4</sub> regeneration from diverse C-1 compounds (Carpenter et al., 2012; Repeta  
87 et al., 2016; Sun et al., 2019). The synergy between autotrophic (e.g., picoeukaryotes, cyanobacteria) and heterotrophic  
88 picoplankton (<3 µm) could represent pathways for CH<sub>4</sub> production in coastal regions. Therefore, the main aim of this study  
89 is to investigate the dynamics of CH<sub>4</sub> oversaturation within the surface layer of the central Chile upwelling zone using  
90 observational and experimental approaches. Among objectives are to discern the contributions of different plankton fractions,  
91 particularly picoplankton and to unravel the involvement of methylated substrates like MPn and TMA in stimulating CH<sub>4</sub>  
92 production. Ultimately, this research will provide comprehensive insights into the biogeochemical mechanisms that drive CH<sub>4</sub>  
93 dynamics within highly productive upwelling water, emphasizing the role of picoplankton in maintaining CH<sub>4</sub> oversaturation  
94 in the surface ocean.

## 95 **2. Material and methods**

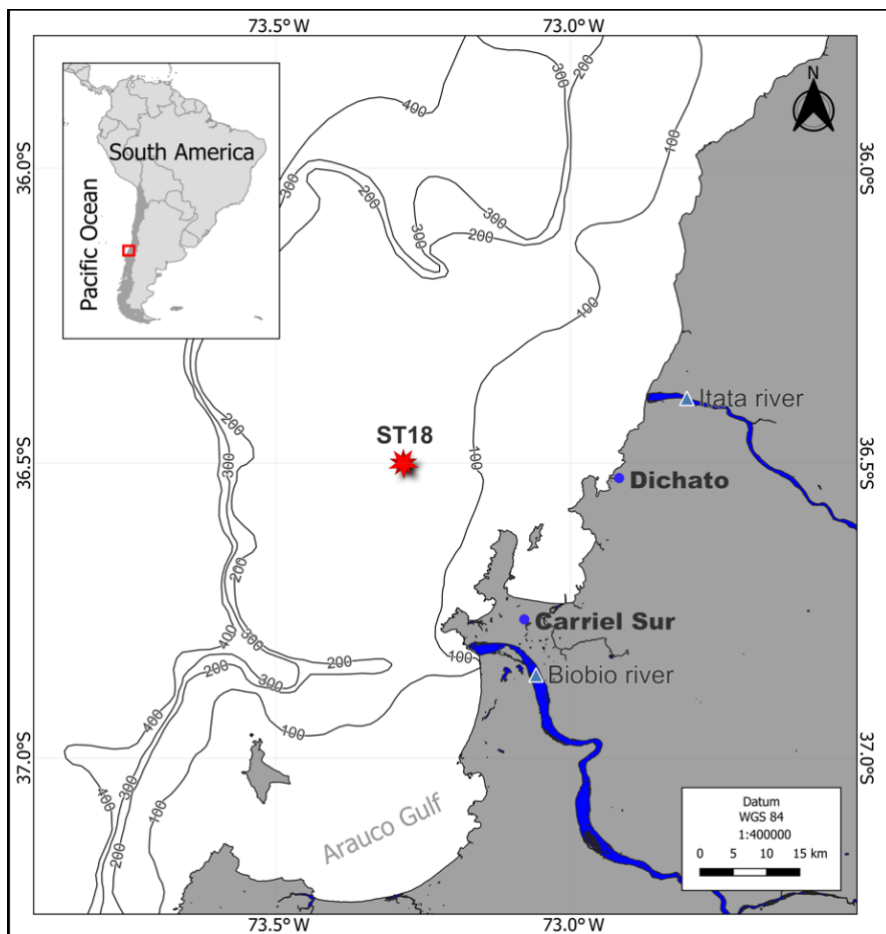
### 96 **2.1 Regional setting.**

97 The continental shelf off central Chile undergoes wind-driven coastal upwelling, seasonally controlled by the migration of the  
98 South Pacific anticyclone (Strub et al., 1998). This process leads to alongshore equatorward winds during the summer- spring  
99 period, producing coastal upwelling (Sobarzo and Djurfeldt, 2004; Sobarzo et al., 2007). The area is influenced by Equatorial  
100 Subsurface Water (ESSW), which is nutrient rich and has low dissolved O<sub>2</sub> levels (less than 44 µM). The ESSW interacts with  
101 sediments and serves as a nutrient source during coastal upwelling, delivering low O<sub>2</sub> concentrations and high organic matter

102 content to the bottom water and sediments, fostering anaerobic organic matter mineralization supporting denitrification,  
103 sulphate reduction and methanogenesis (Ferderlman et al., 1997; Farías et al., 2004).

## 104 2.2 Water collection.

105 Seawater was collected from the upwelling zone of central Chile ( $36^{\circ} 0.802' S$ ;  $73^{\circ} 07.750' W$ ) at the University of  
106 Concepcion's time series station (ST18), situated at a depth of 90 meters (Fig. 1). Monthly samplings have been conducted  
107 aboard the RV Kay Kay II since 2002. Continuous sampling with a CTD-O (SBE-19) instrument was performed to obtain  
108 temperature, salinity, and dissolved oxygen (DO) profiles, whereas seawater samples using 10 L Niskin bottles at various  
109 depths (0, 5, 10, 20, 30, 50, 65 and 80 m) were obtained in triplicate for dissolved gas (DO and  $CH_4$ ), nutrient and chlorophyll-  
110 a (Chl-a) analysis. Detailed methodologies can be found in Farías et al. (2021). From March 2019 to June 2020, DOC samples  
111 were specifically procured from depths of 5, 20, 50 and 80 m.



112  
113 **Figure 1. Time series location map (ST18) over the central Chile upwelling platform. The Itata and Biobio rivers, Carriel sur**  
114 **meteorological station and Dichato town are indicated.**

115 To investigate the role of different sized planktonic communities in CH<sub>4</sub> cycling, seawater was gathered at a depth of 10 m,  
 116 a depth commonly associated with the Chl-a peak (Testa et al., 2018). Large zooplankton (150 µm mesh sieve) were excluded  
 117 using the methodologies outlined by Sieburth et al. (1978). The experimental setup is outlined in Table 1 and includes two  
 118 negative controls: 1) sterile filtration using a 0.2 µm filter, often-used method for the removal of microorganisms (Hahn, 2004),  
 119 and 2) poisoning with the addition of HgCl<sub>2</sub> to ensure total inactivation of few bacterial species which can pass through 0.2-  
 120 microm filters (Hahn, 2004). The positive control was the natural community (NC) without any filtration.  
 121 Another set of experiments enriched with organic methylated substrates as MPn and TMA were performed using only the  
 122 fractionated picoplanktonic community. To maintain the integrity of the samples, the seawater was transported in light- restricted  
 123 black drums under controlled temperature conditions to the Marine Station Biology laboratory at Dichato, minimizing the  
 124 potential for biological activity. This is a time series study, from 2018 until 2021, encompassing CH<sub>4</sub> regeneration in different  
 125 productivity phases (Table 1) according to (Testa et al., 2018).

126 **Table 1. Summary of the experimental setup of short-term (GC vials) and long-term (microcosms) experiments with different**  
 127 **treatments: NC: seawater with the natural plankton (control); <3 µm: picoplankton; <0.2 µm: femtoplankton (control +); <0.2 µm**  
 128 **+ HgCl<sub>2</sub>: femtoplankton with HgCl<sub>2</sub> (control +) and CC: picoplankton concentrate; and the addition of methylated substrates (MPN:**  
 129 **methyl phosphonic acid and TMA: trimethylamines). Different phases of the productivity period are: PI: Phase I; PII: Phase II;**  
 130 **and PIII: Phase III.**

Date	Type of experiment	Setup	Plankton size (µm)	Place	Time (h)	Productivity period
December 2018	GC vials	Plankton fractionation	CN, <3 and <0.2	Incubator	24	High (PI)
January 2019	GC vials	Plankton fractionation	CN, <3 and <0.2	Incubator	24	High (PI)
March 2019	GC vials	Add: MPn	<3	Incubator	24	Intermediate (PII)
May 2019	GC vials	Add: MPn and TMA	<3	Incubator	24	Basal (PIII)
April 2019	Microcosms	Add: MPn and TMA	CN, <3, and CC	Cold room	~ 60	Intermediate (PII)
September 2019	Microcosms	Add: MPn and TMA	CN, <3, and CC	Cold room	~ 60	High (PI)

131

132 **2.3 Short-term experiments of CH<sub>4</sub> cycling from size-fractionated planktonic community enriched with organic**  
133 **substrates.**

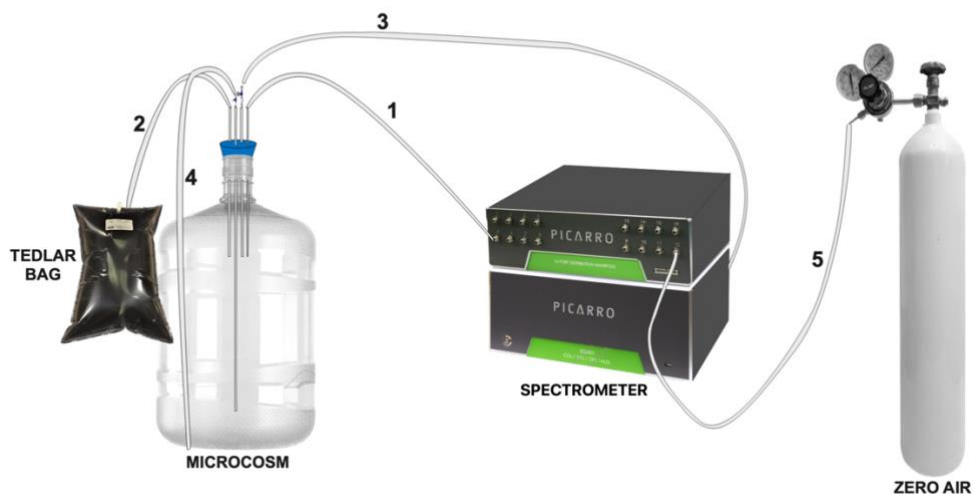
134 The size fractionation of planktonic communities was conducted through a careful sequential filtration process, where 5 L of  
135 seawater was gently passed through a pre-filter of 150 µm nylon, followed by 3 µm Isopore, and 0.22 µm Millipore membranes,  
136 yielding two fractions: picoplankton (<3 µm), and femtoplankton (<0.2 µm) communities; the last one used as a negative  
137 control in some experiments. NC was obtained directly without filtering (Table 1).

138 Prior to incubation, initial seawater sampling was taken for each treatment group, wherein triplicate measurements were taken  
139 of OD (125 mL), COD (60 mL), Chl-a (100 mL), and nutrients (15 mL). Subsequently, each size-fractionated sample was  
140 homogenized and swiftly transferred into 20 mL vials (108 in total, twenty-seven per treatment). These vials were immediately  
141 sealed using rubber and aluminium caps to prevent any potential atmospheric gas contamination. The incubation of these vials  
142 took place within an FOC 225E incubator, maintained at a temperature of 13 °C, and under a 12-hour photoperiod (24 hours).  
143 The illumination was calibrated to fall in a range of 11-11.5 µmol m<sup>-2</sup> s<sup>-1</sup> using blue and neutral density blank filters. At  
144 intervals of four hours, three vials from each treatment (Table 1) were withdrawn, and immediately poisoned with 50 µL of  
145 HgCl<sub>2</sub> and then, the vials were gently agitated to ensure homogenization. Gas chromatography was employed to analyze the  
146 CH<sub>4</sub> content of the vials. In another set of experiments (Table 1), the picoplankton fraction was singled out to ascertain its  
147 capacity for metabolizing methylated substrates and subsequently regenerating CH<sub>4</sub>. This involved adding MPn and TMA to  
148 the samples. The final concentration of both substrates in these treatments was maintained at 1 µM, assuming that natural  
149 concentrations in the seawater were at trace levels. Thus, these could be considered as potential experiments (highly enriched).  
150 The experimental conditions remained consistent with those employed in the earlier experiment.

151 **2.4 Long-term experiments of CH<sub>4</sub> cycling from size-fractionated planktonic community enriched with organic**  
152 **substrates.**

153 Nine microcosms were developed using a system of gas-tight polycarbonate bottles (13 L). Each microcosm contained 10L of  
154 seawater for treatment and 3L of headspace. They were equipped with a closed gas circuit and connected to a gas spectrometer  
155 analyzer capable of simultaneously and continuously measuring various gases, including CO<sub>2</sub>, CH<sub>4</sub>, N<sub>2</sub>O, and humidity  
156 percentage (Fig. 2). Each bottle featured a rubber cap equipped with four holes (as depicted in Fig. 2), housing a 5mm glass  
157 capillary within each hole. These capillaries were connected to gas-tight Teflon hoses. Specifically, the first capillary extended  
158 to the middle of the headspace (1) and was linked to an accessory (16-Port Distribution Manifold A0311) of the Picarro G-  
159 2308 spectrometer for Cavity Ring Spectroscopy System (CRDS), designed for the measurement of gases in equilibrium with  
160 the aqueous phase. The second capillary was suspended within the headspace (2) and connected to a Tedlar bag (3 L) filled  
161 with N<sub>2</sub>. This arrangement aimed to prevent imbalance when drawing water samples from the microcosm. The third capillary,  
162 also suspended in the headspace (3), was equipped with a 3-way cannula, and was connected to the air outlet of the Picarro G-  
163 2308 spectrometer, to facilitate the recirculation of air within the headspace. This system optimization aimed to mitigate  
164 excessive headspace during spectrometer air sampling, preventing a gas-seawater phases imbalance. This hose (3) was

165 adjustable and replaced upon measuring gas concentrations in each microcosm. The fourth glass capillary was submerged in  
166 the seawater, 3 cm from the bottom (4). It was attached to a 3-way cannula, streamlining the sample extraction process.



167  
168 **Figure 2. Assembly of the microcosm for long-term experiments (10 L). Capillary 1 is connected directly to the spectrometer.**  
169 **Capillary 2 is connected to a TEDLAR bag filled with N<sub>2</sub> (3L). Capillary 3 is removable and connected to the outlet of the**  
170 **spectrometer. Capillary 4 is connected to a loose hose for water sampling and hose 5 is connected to zero air.**

171 In both April and September of 2019, a series of long-term microcosm experiments were conducted. These months were  
172 strategically chosen: the first coinciding with the transition of phytoplankton composition to nano-picoplankton (basal  
173 productivity period), and the second with diatom blooms (larger phytoplankton dominance) (high productivity period), as  
174 highlighted in studies by Anabalón et al. (2007) and Cuevas et al. (2004). The experiment encompassed three distinct  
175 treatments, 1) Control without any methylated substrates addition in natural communities (NC), picoplankton community (<  
176 3 µm) and concentrated picoplanktonic community (CC) 2) all treatments enriched with MPn 3) and all treatments enriched  
177 with TMA (see Table 1).

178 The concentrated fraction of picoplankton (CC) was procured through tangential flow filtration via a 0.2 µm filter, following  
179 a procedure developed by Giovannoni et al. (1990) for harvesting greater quantities of microbial biomass and using pre-  
180 filtering steps as discussed earlier to concentrate only picoplankton (<3 µm). To discern whether the tangential flow filtering  
181 was effective, the abundance of cyanobacteria, picoeukaryotes and heterotrophic bacteria was measured with flow cytometry.  
182 The incubations were carried out within a controlled cold room environment, maintaining a temperature range of 12 to 13 °C,  
183 with same illumination used in short periods over 60 hours. In the initial stages, each bottle was sealed and allowed to acclimate  
184 for six hours in darkness. Following this stage, 1 mL of MPn (10 mM stock solution) and TMA (10 mM stock solution) were  
185 introduced to each bottle, yielding a final concentration of 1 µM, matching the conditions established in prior experiments.

186 To prevent CH<sub>4</sub> residue contamination, a purge with Zero air was performed (as shown in Fig. 2, line 5), ensuring accurate  
187 CH<sub>4</sub> concentration measurement within each microcosm, and establishing a baseline. Every four hours a cycle of CH<sub>4</sub>  
188 measurements was conducted continuously over 3 minutes, followed by a 6-minute hose cleaning (used for recirculation) with  
189 Zero air before connecting to capillary 3 for subsequent measurement. It is important to note that the equipment absorbed 240  
190 mL of air per minute of reading. Therefore, air recirculation within the microcosm, as previously mentioned, was essential.  
191 Preceding the actual experiment, the concentrations of gases measured by the spectrometer were closely monitored for 30  
192 minutes, confirming that the recirculation process did not impact the measured gas concentrations.

## 193 **2.5 Chemical and biological analysis.**

### 194 **2.5.1. Dissolved methane.**

195 Once the CH<sub>4</sub> samples were taken, they were stored upside down, at room temperature and protected from light, and then  
196 analyzed in the GC. CH<sub>4</sub> (discrete samples) was determined using the phase equilibrium method (McAuliffe, 1963). In this  
197 procedure, each vial was carefully treated, with the addition of 5 mL of inert gas (helium), creating a headspace to facilitate  
198 equilibrium between the aqueous and gas phases. Subsequently, the gas phase was measured into a gas chromatography  
199 Shimadzu 17 equipped with a flame ionization detector (FID). A Restek RT QS-Bond column (30 m length, 0.53 mm inner  
200 diameter, 20 µm film thickness) was employed, maintained at a temperature of 30 °C with a flow of 2.6 ml min<sup>-1</sup>, using He as  
201 an ultrapure gas carrier.

202 Five-point calibration curves (linear response of the detector) were made for each monthly sample set (treatment), using a gas  
203 with a composition and concentration equivalent to that of the current atmosphere from NOAA (1863.4 ± 0.3 ppbv for CH<sub>4</sub>)  
204 (Bullister et al., 2016) as the primary standard, as well as three standard gas mixtures (Air Liquide, USA) and zero air (synthetic  
205 air without CH<sub>4</sub> tracers). In each CH<sub>4</sub> sample set (every treatment), standards were added at the beginning, middle and end of  
206 the measurements to corroborate the correct functioning of the detector. CH<sub>4</sub> measurements (triplicate) with a variation  
207 coefficient greater than 10% were not considered.

### 208 **2.5.2. Dissolved oxygen.**

209 To assess DO content, 125 mL glass flasks were used for sample collection in triplicate. These samples were immediately  
210 fixed and analyzed within 6 hours of collection through the Winkler method (Carpenter, 1965). The analysis was conducted  
211 using a Dosimat 665 instrument featuring an automatic photometric endpoint detector. The detection limit for this method  
212 stood at 2 µmol L<sup>-1</sup>.

### 213 **2.5.3. Nutrient.**

214 Nutrient samples were collected in triplicate using a 60 mL syringe and filtered through a 0.45 µm cellulose acetate filter. The  
215 filtered content was held in 15 mL Falcon polyethylene bottles and stored at -20°C. Analysis of these nutrient samples followed  
216 standard colorimetric techniques (Grasshoff et al., 1983) and was conducted using a SealAA3 segmented flow auto-analyzer.  
217 This analyzer featured four distinct channels, each equipped with specific modules tailored for individual nutrients.



#### 218 **2.5.4. Chlorophyll-a.**

219 To quantify Chl-a content, triplicate samples of 100 mL seawater were filtered using a GF/F filter and immediately stored at -  
220 20°C. Analysis was performed according to the method outlined by (Holm-Hansen et al., 1965). A Turner Designs 10AU  
221 fluorometer was employed for measurement, and a standard pigment served as a reference (Sigma-Aldrich C6144-1MG).

#### 222 **2.5.5. Dissolved Organic Carbon.**

223 For DOC assessment, samples were collected in triplicate using polyethylene bottles. Each 60 mL seawater sample was filtered  
224 through a GF/F filter that had been pre-treated by heating at 450 °C for 4 hours. After filtration, the samples were acidified to  
225 achieve a pH range of 2-3 and stored at -20 °C. Analysis of these samples involved the infrared combustion method using a  
226 Shimadzu Organic Carbon Analyzer (TOC-LCPH).

#### 227 **2.5.6. Cytometry.**

228 For picoplankton abundance, 3mL of water was fixed with a glutaraldehyde solution (1%) and promptly frozen (-80°C) in  
229 liquid nitrogen for storage. Samples were analyzed with flow cytometry using an INFLUX, Cytopeia, equipped with five lasers  
230 (355-457-488-532-638 nm). Sort gates were optimized based on the autofluorescence of each group. *Synechococcus sp.* were  
231 identified based on their orange fluorescence (530/40 nm) using 488 nm blue and 532 nm green lasers, picoeukaryotes were  
232 identified by their red fluorescence (692/40 nm) using 488 nm blue laser, and bacterioplankton were detected using a  
233 combination of side scatter light (SSC) (related to cell size) versus green fluorescence (530/40 nm).

### 234 **2.6 Data analysis.**

#### 235 **2.6.1. Dissolved methane.**

236 Dissolved CH<sub>4</sub> concentration was calculated using the solubility coefficient from Wiesenburg and Guinasso (1979) the water  
237 column was divided into two layers according to density gradients: (1) surface layer (0 - 20 m) well mixed and (2) subsurface  
238 layer (20 – 90m) from the base of the mixed layer to the bottom, around ~ 90 m (Fariás et al., 2015), this was to interpret the  
239 vertical and temporal variability of CH<sub>4</sub> variation.

#### 240 **2.6.2. Methane saturation.**

241 CH<sub>4</sub> saturation was calculate following Eq. (1):

$$242 \text{ Sat}(\%) = \frac{[\text{CH}_4]_{in\ situ}}{[\text{CH}_4]_{eq}} \quad (1)$$

243 Where [CH<sub>4</sub>]<sub>eq</sub> was calculated using solubility coefficient from Wiesenburg and Guinasso (1979).

#### 244 **2.6.3. Methane anomalies and methane hot moments.**

245 Monthly anomalies of CH<sub>4</sub>, were estimated only in the surface layer, using the following Eq. (2):

$$246 \text{ Anomaly} = \frac{x\text{CH}_4 - \bar{x}\text{CH}_4}{\sigma\text{CH}_4} \quad (2)$$

247 Where: xCH<sub>4</sub> is the discrete value at a certain depth (surface) and time (month), and  $\bar{x}\text{CH}_4$  is the median value for the whole  
248 (2018-2021) period at surface and  $\sigma\text{CH}_4$  is the standard deviation of this dataset. CH<sub>4</sub> hot moments were defined as a  $\Delta\text{CH}_4$   
249 three times higher than the average monthly of anomaly ( $\bar{x} \Delta\text{CH}_4$ ) at each depth within the surface layer as Eq. (3):

250  $\frac{\Delta CH_4}{\bar{x}_{\Delta CH_4}} > 3$  (3)

251 Where:  $\Delta CH_4$  is the disequilibrium of this gas at each depth and was estimated as Eq. (4):

252  $\Delta CH_4 = [CH_4]_{in\ situ} - [CH_4]_{eq}$  (4)

#### 253 **2.6.4. Inventories.**

254 Inventories of  $CH_4$ , Chl-a and nutrients at the surface and subsurface layer were calculate through the trapezoidal integration  
255 of concentrations of each variable at every layer; minimum three depths in each layer. The averages were taken for DOC,  
256 because there were only two measurements in each layer.

#### 257 **2.6.5. Methane recycling rates.**

258 The net  $CH_4$  recycling rate (net  $CH_4$  accumulation minus  $CH_4$  consumption) in different fractions of the phytoplankton  
259 community was calculated through a linear regression of  $CH_4$  concentrations (Farías et al., 2009) during the incubation time  
260 (24 hours), separating the light cycles (12 hours of light and 12 hours of darkness).

#### 261 **2.6.6. Methane fluxes.**

262 The daily  $CH_4$  flux ( $F = \mu\text{mol m}^{-2} \text{d}^{-1}$ ) across air-sea interface was determined using the equation from Broecker and Peng  
263 (1974), modified by Wanninkhof (1992) as follows Eq. (5):

264  $F = K_w * (C_w - C^*)$  (5)

265 Where:  $K_w$  ( $\text{cm h}^{-1}$ ) is the transfer velocity from the surface water to the atmosphere, as a function of wind speed, temperature,  
266 and salinity from the mixed layer depth (MLD), where wind speed were obtained from a meteorological station located at  
267 Carriel Sur (<http://www.meteochile.gob.cl/>) and MLD was calculated using a potential density-based criterion of Kara et al.  
268 (2003).  $C_w$  ( $\text{nmol L}^{-1}$ ) is the mean  $CH_4$  concentration in the mixed layer and  $C^*$  is the gas concentration in the mixed layer  
269 expected to be in equilibrium with the atmosphere according to Wiesenburg and Guinasso (1979). Historical atmospheric  
270 values were obtained from registers of gas hemispheric and global monthly means from the NOAA/ESRL program at NOAA  
271 (<http://www.esrl.noaa.gov>). More details about the calculation of  $CH_4$  fluxes in Farías et al. (2021).

#### 272 **2.6.7. Brunt-Väisälä frequency (BVF).**

273 The Brunt Vaisala frequency was derived from the observed pressures, temperatures and salinities for each depth set using the  
274 TEOS-10 equation of state. This was done in Ocean Data View (ODV v5.6.4) software. Negative values indicate unstable  
275 conditions (Schlitzer, 2023).

### 276 **2.7 Statical analysis**

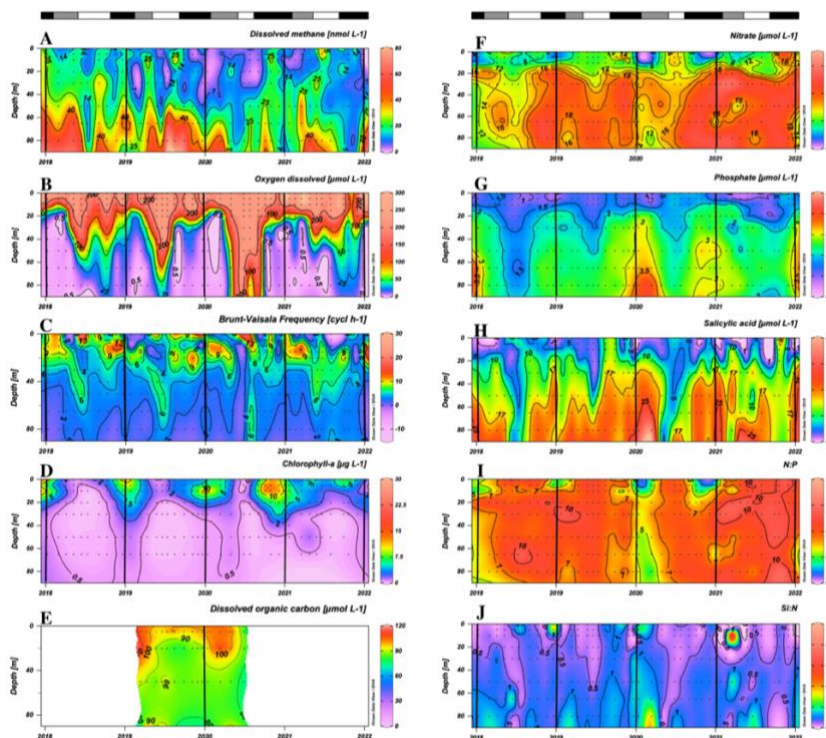
277 To determine significant differences between the upwelling and non-upwelling periods in both surface and subsurface layers,  
278 the non-parametric Mann-Whitney U test was used. To analyse the degree of relationship between oceanographic variables  
279 and the variability of  $CH_4$  in the surface layer, Spearman correlations were used. Also, to identify patterns surface and  
280 subsurface variation, a Principal Component Analysis (PCA) was performed. In addition, the Kruskal-Wallis non-parametric

281 statistical test was used to define significant differences between the concentrations given by the different treatments. The  
282 value statistically significant was considered as  $p < 0.05$ .

### 283 3 Result and discussion

#### 284 3.1 Oceanographic characteristics related to wind-driven coastal upwelling in central Chile.

285 Figure 3 shows the seasonal variability of DO, stratification, Chl-a, DOC, nutrients, and their ratios. Coastal areas off central  
286 Chile have a well-documented seasonality of upwelling favourable winds (Strub et al., 1998). Previous studies, based on wind  
287 forcing, have identified two distinct seasons: spring-summer (September to April) upwelling and fall-winter (May to August)  
288 non-upwelling (Sobarzo et al., 2007). This seasonality significantly influences temperature, salinity, DO, nutrients, and surface  
289 Chl-a concentrations in response to wind-driven stress (Strub et al., 1998; Aguirre et al., 2012). Notably, although most  
290 oceanographic variables have clear seasonal patterns, a comparatively weak seasonality is observed in dissolved  $\text{CH}_4$  (Fig.  
291 3A).



292  
293 **Figure 3. Time series of vertical distributions of A. Methane ( $\text{nmol L}^{-1}$ ), B. Dissolved oxygen ( $\mu\text{mol L}^{-1}$ ), C. Brunt-Vaisala Frequency**  
294 **( $\text{cycl h}^{-1}$ ), D. Chlorophyll-a ( $\mu\text{g L}^{-1}$ ), E. Dissolved Organic Carbon (no Purgeable Organic Carbon -  $\mu\text{M}$ ), F. Nitrate ( $\mu\text{mol L}^{-1}$ ), G.**  
295 **Phosphate ( $\mu\text{mol L}^{-1}$ ), H. Salicylic acid ( $\mu\text{mol L}^{-1}$ ), N:P ratio and J. Si:N ratio. Sampling was made at ST18 from January 2018 to**  
296 **December 2021. Black lines indicate the start of each year (January). The top bars show different periods primary production, in**  
297 **black is a high productivity period (Phase I), in gray is an intermediate productivity period (Phase II), and in white is a low**  
298 **productivity (Phase III).**

299 In the subsurface layer, CH<sub>4</sub> concentrations range from 0.43 to 78.72 nM (mean ± SD = 23.44 ± 15.38 nM, Fig. 3A). These  
300 elevated levels could be associated with the seasonal dynamics of organic matter mineralization under hypoxic and suboxic  
301 conditions during the upwelling period (spring-summer) (Brown et al., 2014; Capelle and Tortell, 2016; Kock et al., 2008;  
302 Farías et al., 2021); however, there are no significant differences in CH<sub>4</sub> accumulations (p = 0.40) in subsurface waters during  
303 the upwelling (mean ± SD = 22.52 ± 14.34 nM) and non-upwelling (mean ± SD = 24.60 ± 16.65 nM) periods (Fig. 3A).  
304 Previously, long-term CH<sub>4</sub> climatology has observed similar values in surface and subsurface layers (Farías et al., 2021).  
305 In the surface layer, there is a highly heterogeneous distribution of CH<sub>4</sub> concentrations, ranging from 0.14 to 41.72 nM (mean  
306 ± SD = 11.70 ± 7.79 nM). There are brief events of high CH<sub>4</sub> accumulations within water column, known as “hot moments”  
307 (McClain et al., 2003; referring to disproportionate accumulations over time). CH<sub>4</sub> concentrations during hot moments are  
308 between 10.17 nM (390% saturation) and 41.72 nM (1650% saturation) and persist during upwelling and non-upwelling  
309 periods, as observed in Fig. S1 and Fig. S2. Persistently high CH<sub>4</sub> concentrations in mixing layer depth results in substantial  
310 CH<sub>4</sub> effluxes, varying between 3.35 and 23.42 μmol m<sup>-2</sup> d<sup>-1</sup> (mean ± SD = 10.10 ± 5.77 μmol m<sup>-2</sup> d<sup>-1</sup>). When effluxes are  
311 estimated and compared for upwelling and non-upwelling periods, there are not significant differences. The lack of seasonal  
312 differences in mean surface CH<sub>4</sub> concentrations (p = 0.63) and effluxes (p = 0.23) could indicate additional input sources, such  
313 as river discharges or local surface production. Potentially, the Itata River may contribute to CH<sub>4</sub>, DOC and chromophoric  
314 DOM (CDOM) discharge (Bello, 2016; Vargas et al., 2016; Rain-Franco et al., 2019); stimulating CH<sub>4</sub> production through  
315 aerobic methanogenesis and photooxidation processes (Li et al., 2020; Zhang and Xie, 2015).  
316 CH<sub>4</sub> profiles from samples are shown in Figure S2. Specific dates present peaks in surface CH<sub>4</sub> over different concentrations,  
317 occasionally presenting levels exceeding those in the subsurface layer; so, it is understood that these hot moments in the surface  
318 layer are not associated with the vertical advection of CH<sub>4</sub>-rich bottom waters.  
319 Thus, it is considered whether hot moments result from physical processes, such as vertical and/or advection associated with  
320 upwelling and river discharge, respectively, or biological microbial processes. For the latter, hot moments might be due to *in*  
321 *situ* aerobic methanogenesis, a process related to the growth and metabolic activities of microalgae (Günthel et al., 2020;  
322 Hartmann et al., 2020; Del Valle and Karl, 2014; Bizic, 2021; Cerbin et al., 2022) and bacteria (Repeta et al., 2016; Metcalf  
323 et al., 2012; Sun et al., 2019). This type of production is suggested to be a significant reason for CH<sub>4</sub> fluxes in various aquatic  
324 systems, including stratified lakes (Grossart et al., 2011; Günthel et al., 2019; Wang et al., 2018), and open oceans (Damm et  
325 al., 2010; Karl et al., 2008; Repeta et al., 2016; Sosa et al., 2020; Ye et al., 2020).  
326 Relatively high Brunt-Väisälä frequency (BVF) values (>10 cycl/h) are observed between depths of 0 and 20 m, particularly  
327 from September to December (Fig. 3C), whereas subsurface BVF values seem to be associated with annual patterns of thermal  
328 stratification, where upwelling from the nearly homogenous ESSW between October and April leads to high density  
329 homogeneity and lower BVF values. During fall and winter, elevated BVF values are observed in surface waters, probably  
330 due to discharge from the Itata river; remarkably there are notably stable values in the subsurface layer (Fig. 3C).  
331 The upper 20 m of the water column has Chl-a concentrations above 10 μg L<sup>-1</sup> (with a marked subsurface peak over different  
332 depths) (mean ± SD 6.60 ± 5.98) in September to January (spring-summer); while lower and more homogeneous values

333 (ranging from 0.5 to 1  $\mu\text{g L}^{-1}$ ) are detected during late summer (February to April, mean  $\pm$  SD  $3.23 \pm 2.87$ ), fall and winter  
 334 (May to August, mean  $\pm$  SD  $1.36 \pm 1.91$ ) (Fig. 3D). The study area presents typical DOC concentrations, as expected for  
 335 highly productive coastal zones (Igarza et al., 2019; Vargas et al., 2013), ranging from 58.79 to 128.63  $\mu\text{M}$  (mean  $\pm$  SD =  
 336  $90.37 \pm 17.05$ ) with peak DOC concentrations during late summer and early fall (Fig. 3E). The surface layer shows reduced,  
 337 but not depleted nutrient concentrations, whereas the subsurface layer presents consistently higher nutrient concentrations (Fig.  
 338 3F–H). Within the upper 10 m depth, minimum mean  $\text{NO}_3^-$  and  $\text{PO}_4^{3-}$  concentrations occur from September to January, and  
 339 intermediate and higher values between February and August (Fig 3 F–G). These trends are consistent with plankton temporal  
 340 dynamics (see below). In contrast,  $\text{Si(OH)}_4$  exhibits higher but heterogeneous concentrations during late autumn and winter,  
 341 and lower values during spring and summer (Fig. 3H). This pattern reflects the high levels of  $\text{Si(OH)}_4$  associated with river  
 342 discharges in winter and the development of diatom blooms in spring and summer.  $\text{CH}_4$  hot moments occur consistently  
 343 throughout the year with different stratification scenarios in the water column (Fig. 3A and C), and with different Chl-a levels  
 344 (Fig. 3D), revealing a complex interaction between substrates (nutrients and DOC), involved microorganisms and  
 345 environmental factors (e.g. light, nutrients, water column stability).

346 Three distinct periods or phases of annual productivity are considered within the study area, based on existing data of primary  
 347 production, phytoplankton biomass, and phytoplankton succession (i.e. changes in composition), related with other biophysical  
 348 variables (Testa et al., 2018). These periods are; September to January (Phase I), with high productivity and Chl-a biomass,  
 349 dominated by microplankton including large diatoms, tintinids, and dinoflagellates; from February to April (Phase II) with  
 350 intermediate productivity, characterized by a shift in plankton composition biomass from larger to smaller organisms, such as  
 351 flagellates; and from May to August (Phase III), with basal level productivity and relatively low Chl-a biomass, which  
 352 corresponds to a non-upwelling period, with a prevalence of pico and nanoplankton (e.g., *Synechococcus*) including small  
 353 flagellates and ciliates.

354 Table 2 presents inventories on  $\text{CH}_4$ , Chl-a, DOC,  $\text{NO}_3^-$ ,  $\text{PO}_4^{3-}$ ,  $\text{Si(OH)}_4$ , and inorganic nutrient ratios (N:P and Si:N) observed  
 355 in these periods. The data on Chl-a indicates a marked variation, decreasing from spring to winter (Table 2).

356 **Table 2. Average inventories of biogeochemical variables: methane ( $\mu\text{mol m}^{-2}$ ), chlorophyll-a ( $\text{mg m}^{-2}$ ), DOC ( $\mu\text{mol m}^{-2}$ ), nitrate**  
 357 **( $\mu\text{mol m}^{-2}$ ), phosphate ( $\mu\text{mol m}^{-2}$ ), silicate ( $\mu\text{mol m}^{-2}$ ), N:P and Si:N ratios, estimated for each productivity period (mean  $\pm$  SD) from**  
 358 **2018 to 2021. These inventories are estimated for surface (SL) and subsurface layer (SSL). Number of hot moments in each period**  
 359 **are counted. Phase I: September to January. Phase II: February to April. Phase III: May to August.**

Variable	Layer	Productivity periods		
		High	Intermediate	Basal
		Phase I (spring-summer)	Phase II (summer-autumn)	Phase III (autumn-winter)
$\text{CH}_4$	SL	$265.59 \pm 58.36$	$162.35 \pm 21.44$	$240.54 \pm 78.97$
	SSL	$1315.07 \pm 173.69$	$1012.86 \pm 163.23$	$1275.17 \pm 286.38$

Chl-a	SL	154.4 ± 102.31	51.32 ± 31.02	26.19 ± 21.17
DOC	SL	114.44 ± 53.94	112.88 ± 8.36	92.41 ± 11.27
	SSL	100.35 ± 46.51	96.97 ± 23.78	86.12 ± 8.95
NO <sub>3</sub> <sup>-</sup>	SL	260.61 ± 96.25	208.67 ± 49.51	224.65 ± 13.44
	SSL	1274.41 ± 344.24	1033.51 ± 38.5	987.6 ± 113.58
PO <sub>4</sub> <sup>-3</sup>	SL	38.08 ± 10.35	30.29 ± 3.51	28.16 ± 2.99
	SSL	170.22 ± 34.07	137.05 ± 21.57	119.38 ± 11.73
Si(OH) <sub>4</sub>	SL	131.75 ± 47.07	91.65 ± 38.68	111.24 ± 37.9
	SSL	1065.32 ± 206.98	811.2 ± 225.51	678.07 ± 168.68
N:P	SL	7.69 ± 2.57	7.59 ± 2.44	8.48 ± 0.55
	SSL	9.28 ± 2.52	8.24 ± 0.92	8.46 ± 0.84
Si:N	SL	0.67 ± 0.1	0.69 ± 0.73	0.49 ± 0.15
	SSL	1.04 ± 0.08	1.01 ± 0.26	0.74 ± 0.11
Hot moments	SL	19	9	15

360

361 Notably, surface data on DOC shows a marginal reduction from Phase I to Phase III (Table 2). It is possible that this fluctuation  
362 in DOC accumulation/depletion is due to the microbial regeneration exceeding the heterotrophic bacterial consumption  
363 (Hansell and Orellana, 2021), or it attributes to allochthonous sources from rivers (Bauer and Druffel, 1998). Nutrient  
364 distribution and concentrations in the surface layer show significant variability among phases (Fig. 3F, G, and H) due to the  
365 varied influence by nutrient-rich upwelling events (predominantly observed in spring-summer), biological assimilation and  
366 river discharge. These variations significantly affect the N:P and Si:N ratios (Fig. 3I and J), potentially influencing  
367 phytoplankton composition. During winter (Phase III), the N:P ratio approaches the expected Redfield stoichiometry, attributed  
368 to reduced denitrification in bottom waters (Fernandez et al., 2015) and limited vertical advection towards the surface,  
369 contrasting with Phase I. Simultaneously, the Si:N ratio increases due to freshwater discharge from the Itata River (Phase III),  
370 encouraging an increase in large diatoms and subsequent Si(OH)<sub>4</sub> consumption (Phase I). Considering that hot moments occur  
371 throughout different phases and stages of primary production, as well as phytoplankton composition succession (Collado-  
372 Fabbri et al., 2011; Aldunate et al., 2018; Anabalón et al., 2007), various levels of Chl-a (see Table 2), and under different  
373 nutrient ratios and DOC concentrations (Table 2), it suggests that the conditions and processes favouring the occurrence of hot  
374 moments are variables and not entirely clear.

375 The correlation analysis in the water column showed no significant correlations between CH<sub>4</sub> and the other physicochemical  
376 variables (Fig. S3A), however nutrients such as PO<sub>4</sub><sup>-3</sup> were significantly correlated with T (negative correlation), S (positive  
377 correlation), DO (negative correlation) and Si:N ratio (positive correlation) (Fig. S3A), which may be associated with the  
378 nutrient-rich, oxygen-poor of the ESSW. When the surface layer was analyzed in the three productivity periods (Fig. S3B, C  
379 and D), again, no correlation was observed between CH<sub>4</sub> and the other biogeochemical variables, however, in the phase I and

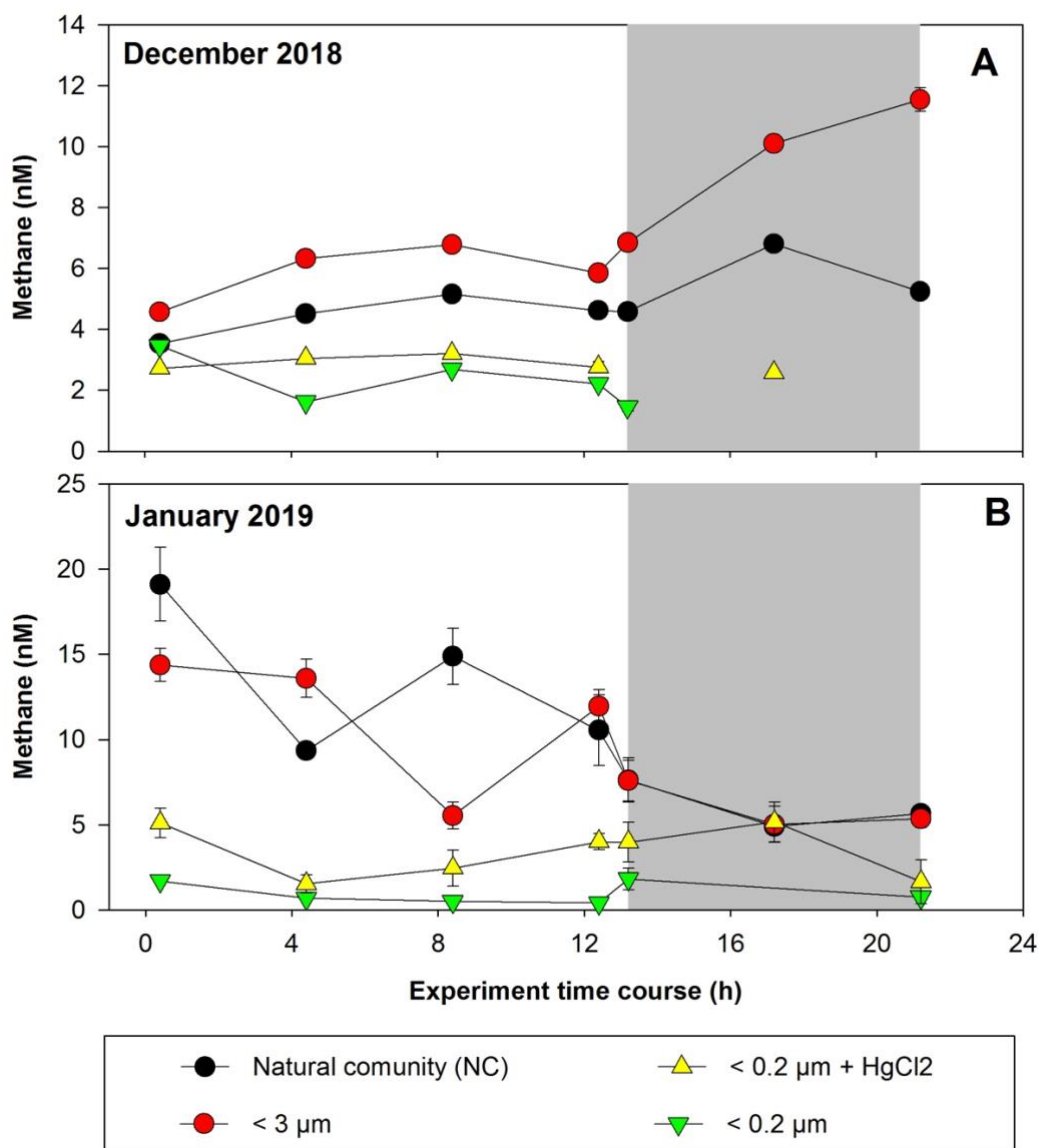
380 II, significant correlations are observed between the nutrients and T, S and DO (negative correlations) (Fig. S3B and C), which  
381 may be associated with the upwelling during spring-summer. In the phase III (Fig. S3D), only  $\text{Si}(\text{OH})_4$  showed significant  
382 correlations with T (negative correlation),  $\text{NO}_3^-$  (positive correlation),  $\text{PO}_4^{3-}$  (positive correlation) and the Si:N ratio (positive  
383 correlation), this may be due to Si input during the rainfall period presented in the autumn-winter period. Moreover, the slight  
384 correlation (but no significant) between  $\text{CH}_4$  and Chl-a in Phase III, suggests the possibly organic matter  
385 degradation/consumption could impact  $\text{CH}_4$  production and that low scale processes (order of hours or days) could mask this  
386 correlation, since there is a wide range in the composition of the phytoplankton species are involved in  $\text{CH}_4$  cycling (Klitzsch  
387 et al., 2019, 2023; Günthel et al., 2020).

388 We further explore the multivariate relationship between  $\text{CH}_4$  variability and other variables by separating the data into the  
389 surface and subsurface layers by performing a PCA (Fig. S3). Although the  $\text{CH}_4$  vector contributes minimally to the total  
390 variance in the dataset, distinct behaviour is observed in both layers (Fig. S3). In the surface layer, Principal Component 1  
391 (PC1) shows almost no variability in  $\text{CH}_4$  and accounts for 25% of the total variance. PC2 contains 22.1% of the total variance  
392 and reveals a direct relationship between  $\text{CH}_4$  and the variables Chl-a, primary production, Si:N ratio,  $\text{Si}(\text{OH})_4$ ,  $\text{PO}_4^{3-}$ , and  
393  $\text{NO}_3^-$ , while being negatively correlated with temperature, DO,  $\text{NO}_2^-$ , and N:P ratio. When separating dataset into phases, there  
394 are differences in variability and the components. Surface variability is highest in Phase I and lowest in Phase III. Phases I and  
395 II vary on both axes, while Phase III is mainly contained on PC2. For the subsurface, the variability is similar in all phases,  
396 but the components on which the variability occurs are more differentiated. Phase III varies almost exclusively in the first  
397 dimension (the point cloud aligns along the x-axis), while Phases I and II vary on both dimensions (the point cloud is oblique  
398 to the axes), this may be due to the differentiation between the upwelling (Phases I and II) and non-upwelling (Phase III)  
399 periods.

400 So, the complexity inherent in  $\text{CH}_4$  dynamics within the study area poses a challenge to comprehension. Consequently, both  
401 short- and long-term  $\text{CH}_4$  cycling experiments have been conducted to enhance our understanding. These experiments  
402 specifically target size-fractionated planktonic communities combined with organic substrates. The objective is to unravel the  
403 intricate interactions and substrates that potentially influence  $\text{CH}_4$  production. By focusing on size fractions within planktonic  
404 communities, it is possible to assess the contribution of diverse groups to  $\text{CH}_4$  production.

### 405 **3.2 Short-term $\text{CH}_4$ cycling within size fractionated planktonic communities.**

406 Figure 4 shows  $\text{CH}_4$  accumulation/depletion in plankton-fractionated experiments over a timeframe, with daily incubations  
407 (12 hours of light and 12 hours of darkness). Initial experiments were conducted in December 2018 (Fig. 4A) and January  
408 2019 (Fig. 4B), corresponding to a period of high productivity or Phase I (Table S1) and coinciding with strong vertical  
409 advection. The surface water exhibits cooling ( $\sim 12\text{-}13^\circ\text{C}$ ) and elevated  $\text{CH}_4$  levels (9.44–17.09 nM), indicative of an active  
410 upwelling period (Farías et al., 2021), aligning with other indicators of coastal upwelling (Aguirre et al., 2021).



411

412 **Figure 4. Time courses of dissolved methane concentration (nM) during incubations with fractionated plankton experiments (NC: natural community; <3 μm: picoplankton and controls (<0.2 μm)). A. December 2018 and B. January 2019. Photoperiod is represented in white (light) and gray (dark). Error bars represent standard deviation of triplicate samples, when error bars are not visible, they are within the area of the symbol.**

416

In the treatments involving fractions <0.2 μm and <0.2 μm + HgCl<sub>2</sub>, which serve as negative controls, CH<sub>4</sub> concentrations remain relatively constant during incubation, with concentrations below 2.32 nM (Fig. 4A) and 5.51 nM (Fig. 4B), indicating biological CH<sub>4</sub> production (Table S2). However, abiotic CH<sub>4</sub> production via photooxidation of CDOM may occur (Li et al., 2020; Zhang and Xie, 2015), but this is not considered in this study. Processes such as DOM photochemical reactions (Mopper

419



420 et al., 2015), which can contribute to the DOM pool at shallower depths (<10 m) and be photo-oxidized to produce CH<sub>4</sub>, are  
421 disregarded under natural conditions (Li et al., 2020; Zhang and Xie, 2015). In December, CH<sub>4</sub> concentrations in the NC  
422 (positive control) and <3 μm fractions undergo slight increases under light conditions (Fig. 4A, Table S2). However, during  
423 darkness, the net CH<sub>4</sub> accumulation is significantly higher in the <3 μm fraction (p = 0.03; Table S2). Picoplankton includes  
424 autotrophic and heterotrophic unicellular organisms in the size range of 0.2 to 2 μm. The autotrophic organisms comprise  
425 cyanobacteria (*Prochlorococcus* and *Synechococcus*) and diverse picoeukaryotes larger than 1 μm (Worden, 2006), while the  
426 heterotrophic organisms are primarily prokaryotes, with bacteria overwhelmingly dominating over archaea in the upper layers  
427 (Smith et al., 2013). This fraction (<3 μm) includes several coexisting metabolic groups that depend on different energy sources  
428 such as sunlight, DOC, or even a combination of the two (mixotrophy). These groups are critical for the functioning of the  
429 microbial food web and are predominantly responsible for DOC cycling (Muñoz-Marín et al., 2020; Reintjes et al., 2020) and  
430 its derivative compounds (including CH<sub>4</sub>).

431 In January, the experiments show distinct results, with CH<sub>4</sub> levels decreasing over incubation time in both the NC and <3 μm  
432 fractions for both photoperiods (Fig. 4B), although the rate of consumption is lower in darkness (Table S2). These differences  
433 suggest that the composition of the microbial community during the high productivity period, as well as the quantity and  
434 quality of DOC and nutrient concentrations and their ratios (Allen et al., 2012; Spilling et al., 2019), control CH<sub>4</sub> cycling.  
435 Indeed, the environmental conditions differ during sampling (Table S1); although both months are oxygenated, both vary in  
436 Chl-a and nutrient levels, including CH<sub>4</sub> (Fig. 3C; Table S1).

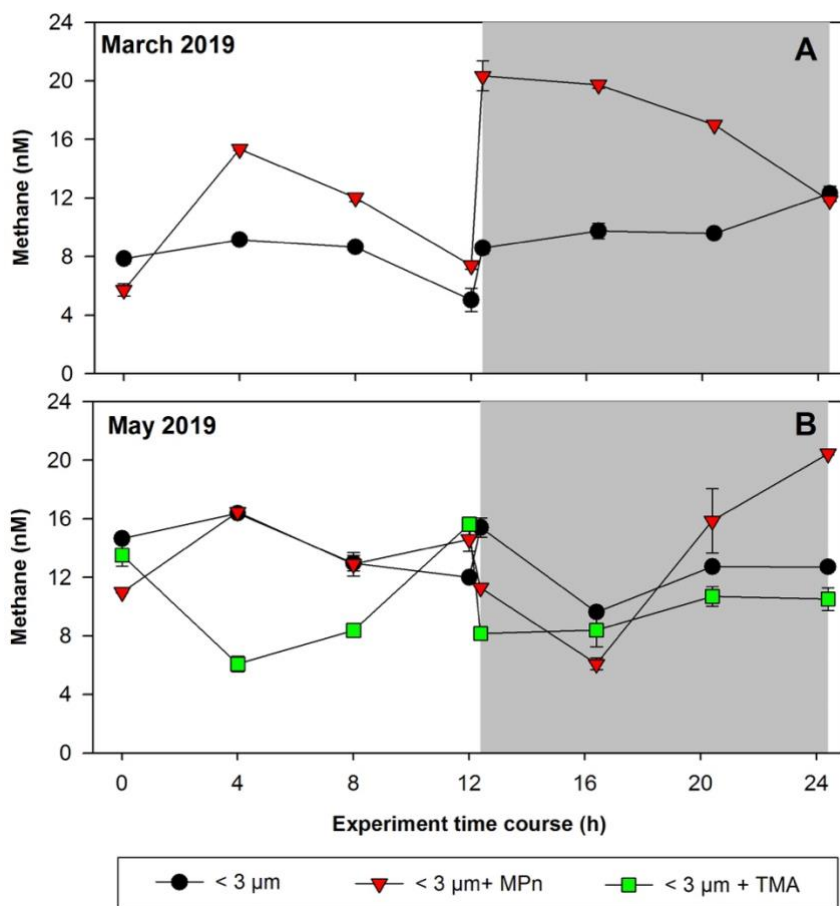
437 Significant differences in CH<sub>4</sub> accumulation rates between the NC and <150 μm fraction treatments (data not shown) are  
438 observed compared with the <3 μm fraction (Table S2). Peak cycling rates occur in the <3 μm fraction, indicating that larger  
439 microorganisms do not affect the net CH<sub>4</sub> accumulation/consumption (Table S2), highlighting the importance of the microbial  
440 loop in CH<sub>4</sub> cycling. Additionally, the observed differences between photoperiods in both fractions may suggest coupling  
441 mechanisms between autotrophic phytoplankton and heterotrophic bacterioplankton communities (León-Palmero et al., 2020;  
442 Morán et al., 2002; Repeta et al., 2016).

443 CH<sub>4</sub> consumption by methanotrophs should be considered in CH<sub>4</sub> cycling experiments, as aerobic CH<sub>4</sub> oxidation significantly  
444 reduces the net CH<sub>4</sub> accumulation rates (net production vs. consumption) (Mao et al., 2022). While the impact of light on  
445 methanotrophs is not widely understood (Broman et al., 2023), existing literature suggests that methanotrophs may experience  
446 inhibition under light conditions (Dumestre et al., 1999; Morana et al., 2020). Consequently, CH<sub>4</sub> accumulation should be  
447 higher under these conditions. However, this does not agree with our results (for light/dark conditions), indicating that  
448 methanotrophs are more dynamic and complex than expected, making them difficult to understand through the observation of  
449 their daily cycles.

### 450 **3.3 Short-term CH<sub>4</sub> cycling experiment from picoplankton amended with organic substrates.**

451 As the picoplankton fraction showed the highest rate of CH<sub>4</sub> accumulation (Fig. 4), this prompts its selection for assessing its  
452 potential for methylotrophic methanogenesis through the addition of methylated substrates (MPn and TMA) in a daily cycle.

453 Phosphonate (MPn) and methylamines compounds (mono, di and trimethylamines) are dissolved methylated compounds  
454 known to stimulate CH<sub>4</sub> production because they have a methyl radical (-CH<sub>3</sub>), a potential precursor for CH<sub>4</sub> formation in  
455 oxygenated environments (Karl et al., 2008; Repeta et al., 2016; Wang et al., 2021; Bižić-Ionescu et al., 2018).  
456 These compounds are ubiquitous in various ecosystems (Lohrer et al., 2020; Sun et al., 2019), yet they have distinct metabolic  
457 origins. The MPn originates from microorganisms as Arquea *Nitrosopumilus maritimus* (Metcalf et al., 2012) and is found at  
458 very low concentrations (~0.01 μM, close to its analytical detection limit) likely due to rapid microbial turnover (Karl et al.,  
459 2008; Martínez et al., 2013; Urata et al., 2022). The methylamines compounds as the trimethylamine compounds exhibit a  
460 wide concentration range in the ocean, from nM levels in the open ocean to μM levels in sediments and near the coast (Sun et  
461 al., 2019). Environmental TMA concentrations could be higher, particularly in upwelling that bring the TMA from bottom  
462 waters to the surface (Gibb et al., 1999; Sun et al., 2019). In this context, the amendments performed for each substrate, 100-  
463 fold for MPn and 1000-fold for TMA, convert these experiments into potential rates.  
464 These amendment experiments were conducted in Phase II (March 2019) and Phase III (May 2019), periods of change in  
465 phytoplankton succession (composition), biomass and abundance (Testa et al., 2018). In winter, the relative abundance of  
466 picoplankton with respect to microplankton (particularly the presence of *Synechococcus* and nitrifying archaea) increases  
467 significantly, especially photosynthetic picoeukaryotes (Collado-Fabbri et al., 2011). The time course CH<sub>4</sub> accumulation  
468 during incubations is illustrated in Fig. 5. The highest CH<sub>4</sub> accumulation are observed in the MPn-amended treatment,  
469 particularly under dark conditions in May (Phase III) (Fig. 5B; Table S1). Interestingly, in both periods, the <3 μm + MPn  
470 treatment exhibits contrasting patterns under dark conditions (Fig. 5A and 4B), decreasing in Phase II, and increasing in Phase  
471 III and suggesting the importance of microbial composition. During winter, a higher DOC concentration is observed (Fig 3E),  
472 which may lead to higher bacterial and archaeal activity that could be metabolizing DOC, including MPn under dark  
473 conditions.



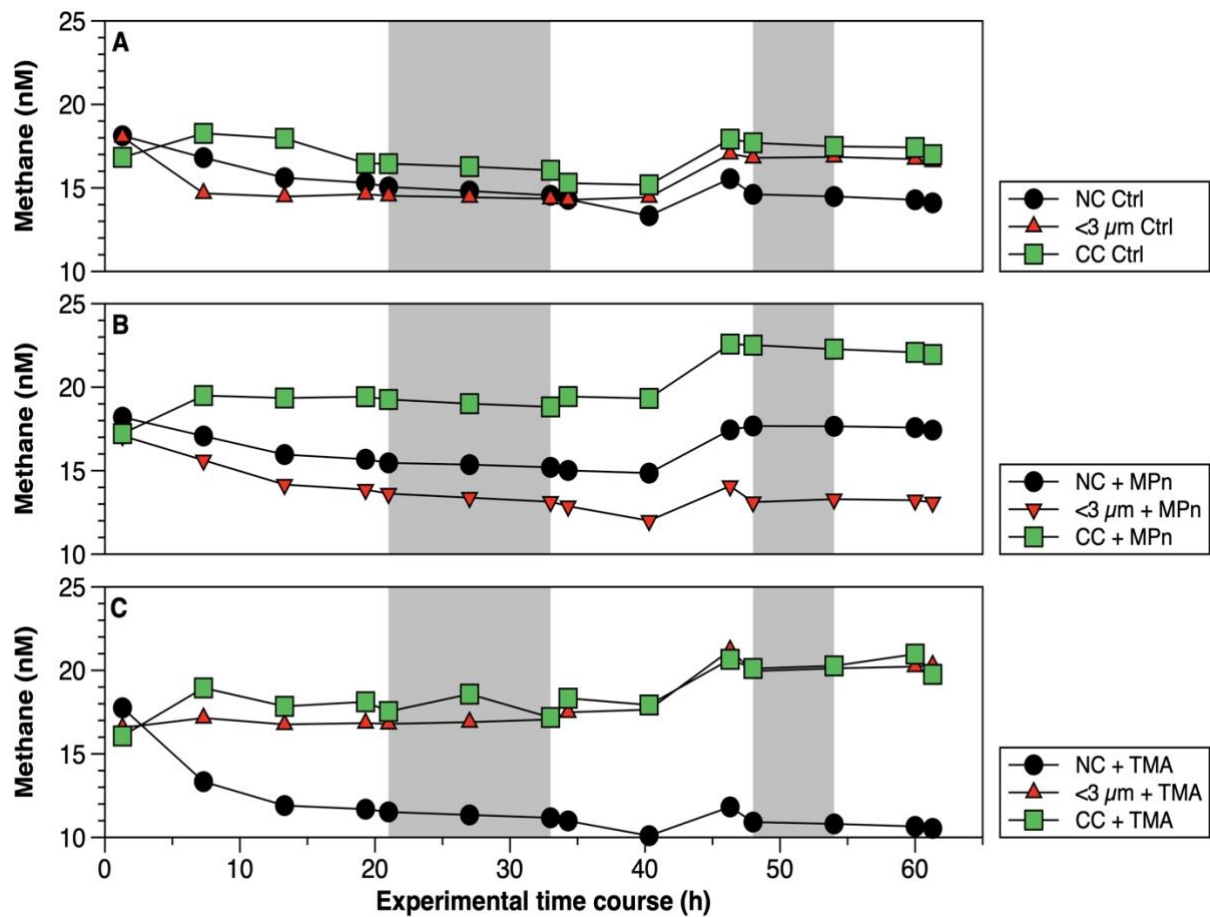
474  
 475 **Figure 5.** Time courses of dissolved methane concentration (nM) during incubations with the addition of methylated substrates  
 476 (MPn: methyl phosphonic acid and TMA: trimethylamine) performed with bacterioplankton (<3 μm) and bacterioplankton  
 477 concentrate (CC). A. March 2019 and B. May 2019. Photoperiod is represented in white (light) and gray (dark). Error bars represent  
 478 standard deviation of triplicate samples, when error bars are not visible, they are within the area of the symbol.

479 Conversely, the TMA treatment does not result in any CH<sub>4</sub> accumulation, being lower compared to the control and MPn  
 480 treatments (Fig. 5B); while TMA can be metabolized by marine bacteria (Lidbury et al., 2015; Bižić-Ionescu et al., 2018), the  
 481 lower CH<sub>4</sub> production in this treatment suggests a different outcome. In contrast, heterotrophic picoplankton might metabolize  
 482 MPn and produce CH<sub>4</sub>, showing *in situ* methanogenesis via the carbon-phosphorus (C-P) lyase pathway (Karl et al., 2008).

### 483 3.4 Long-term CH<sub>4</sub> cycling from concentrated picoplankton amended with organic substrates.

484 For a more comprehensive understanding, our study involves long-term microcosm experiments conducted during two distinct  
 485 phases of productivity. One of these phases occurs during intermediate productivity (Phase II or late summer to autumn),  
 486 characterized by a notable prevalence of autotrophic small diatoms, pico-eukaryotes, and cyanobacteria (*Synechococcus*), in

487 contrast to the high productivity period (Phase I or early springtime) (Fig. S5A and D), where large diatoms are predominant  
488 (Fig. S5B and E), while heterotrophic bacterioplankton exhibits an almost constant presence in both periods (Fig. S5C and F).  
489 These temporal distributions align with well-documented phytoplankton and bacterioplankton patterns in our study area  
490 (Aldunate et al., 2018; Collado-Fabbri et al., 2011; De La Iglesia et al., 2020; Molina et al., 2020).  
491 Briefly, Flavobacteraceae, SAR11 subclade IA (*Candidatus Pelagibacter ubique*-associated), SAR11 subclade 1b,  
492 gammaproteobacterial clades, and SAR86 are prevalent during upwelling seasons, while during non-upwelling seasons or  
493 Phase III, SAR11 subclade II, Marine Actinobacteria, and unclassified Alphaproteobacteria dominate (Aldunate et al., 2018).  
494 In addition, photosynthetic picoplankton eukaryotes related to Mamiellophyceae (*Bathycoccus*, *Micromonas*, and  
495 *Ostreococcus*) are predominantly observed with high significance in the surface layer during the transition period (Collado-  
496 Fabbri et al., 2011; De La Iglesia et al., 2020), whereas the abundance of heterotrophic bacteria, ranging from 0.23 to 6.50  
497  $\times 10^6$  cells  $\text{mL}^{-1}$ , is mainly concentrated in the surface during late summer and autumn, with minima in winter (Molina et al.,  
498 2020). However, in our study, the abundance of heterotrophic bacteria shows no significant differences ( $p = 0.05$ ) in both  
499 periods ( $1 \times 10^6$  cells  $\text{mL}^{-1}$ ) (Fig. S5C and F). This is due to the low DOC at the beginning of the upwelling period (Fig. 3E).  
500 The  $\text{CH}_4$  accumulations during time incubations under different treatments in Phase II are illustrated in Figure 6. The  
501 concentrated community (CC) results in substantial enrichments of cyanobacteria (*Synechococcus*), picoeukaryotes, and  
502 heterotrophic bacteria by factors of 1.9, 1.8, and 4.6, respectively, compared to the NC, and factors of 1.8, 1.8, and 6.1,  
503 respectively, in relation to the natural  $<3 \mu\text{m}$  fraction (Figure S5A, B, and C). In both cases, a significant increase in bacteria  
504 is observed (Figure S5C). The microbial abundance proportions in the NC treatment at the beginning of the experiment closely  
505 align with field observations (Collado-Fabbri et al., 2011; Anabalón et al., 2007; Morales et al., 2007).  
506



507  
 508 **Figure 6.** Time courses of dissolved methane (nM) during incubation in long-term microcosm experiments (10L) with the addition  
 509 of methylated substrates (MPn: methyl phosphonic acid and TMA: trimethylamine) performed with three planktonic communities  
 510 (NC: natural community; <3 μm: bacterioplankton and CC: community concentrate) under oxygenated conditions in April 2019.  
 511 Photoperiod is represented in white (light) and gray (dark).

512 Mean Chl-a levels in the <3 μm fraction are 21.7 and 4.5 times lower than in the NC and CC, respectively (Table S3). This  
 513 suggests that this fraction contains phyto-picoeukaryotes (e.g., coccolithophorids, cryptophytes) and picocyanobacteria (e.g.,  
 514 *Synechococcus*) in a lower proportion than the CC. Additionally, the CC treatment displays higher background levels of DOC  
 515 and nutrients probably due to the natural diurnal mortality of picoplankton (Llabrés et al., 2011). It cannot be ruled out that the  
 516 baseline is due to tangential flow filtration, although it is one of the most used methods to concentrate DOM (Benner et al.,  
 517 1992), reducing the amount of membrane sorption and fouling (Minor et al., 2014). When comparing the treatments (NC, <3  
 518 μm, and CC) without (controls) and with the addition of MPn and TMA (Fig. 6), although temporal patterns are similar,  
 519 significant differences between treatments ( $p = 0.002$ ) are found with slightly higher CH<sub>4</sub> accumulation during the second  
 520 photoperiod, especially in the CC and <3 μm fractions (Fig. 6A). This suggests that during the first photoperiod, there may be  
 521 changes and/or acclimation of planktonic communities.

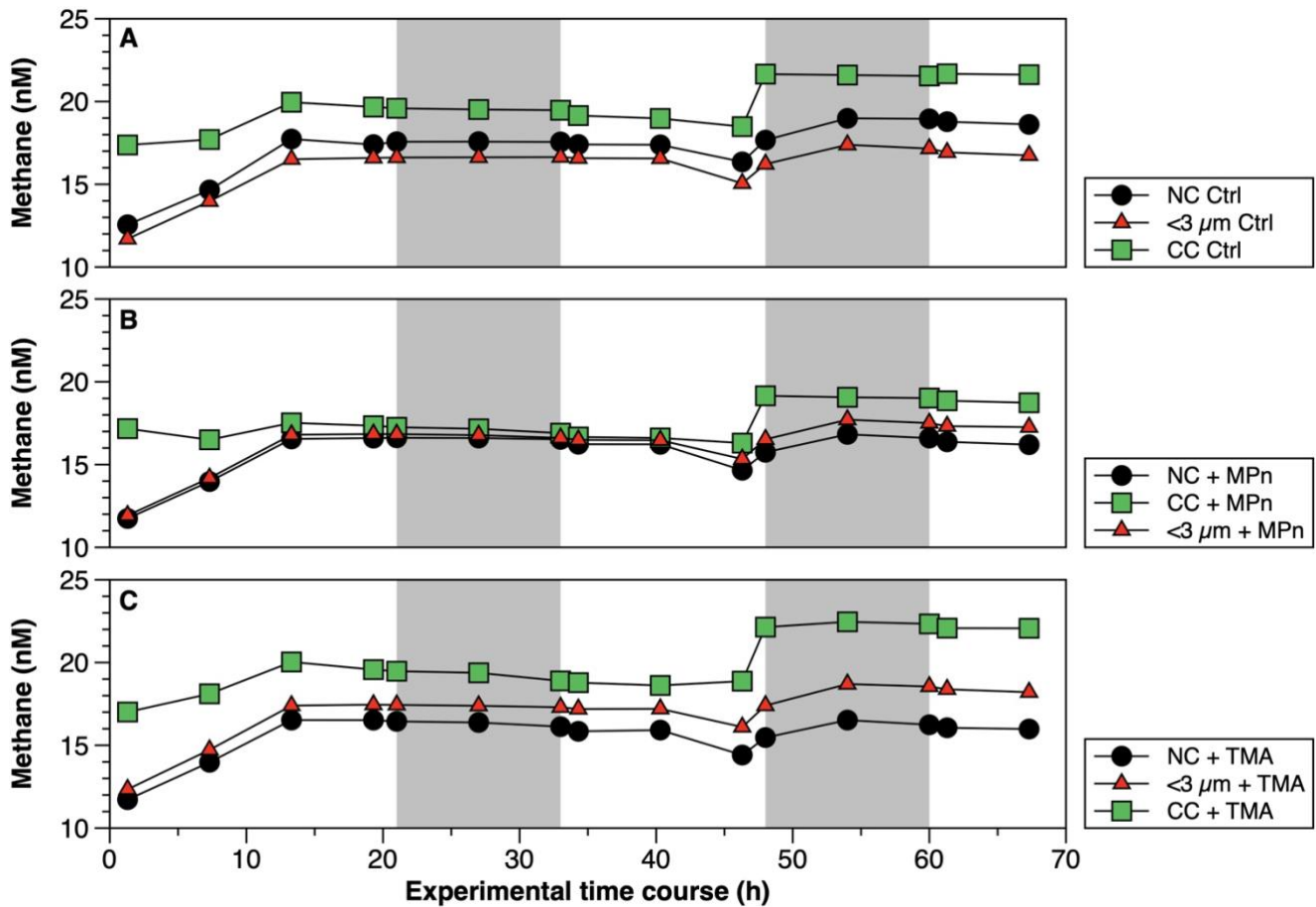
522 With the addition of MPn (Fig. 6B), the CC+MPn treatment, characterized by the highest abundance of autotrophic  
523 (cyanobacteria) and heterotrophic microorganisms (Fig. S5), exhibits a significant increase in CH<sub>4</sub> accumulation. In addition,  
524 higher Chl-a concentrations (Table S3) in the NC treatment may have supported greater CH<sub>4</sub> accumulation compared to the  
525 <3 μm fraction (Fig. 6B). Regarding the TMA enrichment (Fig. 6C), both the CC and the <3 μm fraction treatments respond  
526 similarly, increasing CH<sub>4</sub> concentration over time ( $p = 3 \times 10^{-6}$ ; Fig. 6C) and suggesting that microbial abundance does not  
527 significantly affect CH<sub>4</sub> production with TMA or that the heterotrophic community in the CC treatment weakly metabolizes  
528 TMA (De Angelis and Lee, 1994; Bižić-Ionescu et al., 2018).

529 Although the metabolization of methylated substrates, such as MPn to CH<sub>4</sub> by various types of bacteria, has been extensively  
530 documented (Repeta et al., 2016; Del Valle and Karl, 2014; Metcalf et al., 2012; Zhao et al., 2022; Damm et al., 2010; Karl et  
531 al., 2008), this has only been reported mostly under phosphorus-starved conditions. However, this is unlikely in our study area,  
532 which experienced high PO<sub>4</sub><sup>-3</sup> availability, even in excess compared to N (Table 2). Specifically, the expression of phosphonate  
533 C-P lyase genes could arise when P-starved (Carini et al., 2014; Taenzer, 2019; Sosa et al., 2019). Thus, an alternative  
534 explanation for the significant CH<sub>4</sub> accumulation in the CC with MPn treatment could be related to the presence of  
535 photosynthetic cyanobacteria (Bižić et al., 2020).

536 Given that *Synechococcus* dominates during the non-upwelling period (autumn-winter season) in the photic layer (Collado-  
537 Fabbri et al., 2011), it becomes plausible to consider CH<sub>4</sub> production mediated by this microorganism in our upwelling system.  
538 Consequently, CH<sub>4</sub> production pathways appear multifaceted, involving complex interplays between photochemical and  
539 metabolic processes. The mechanism by which cyanobacteria effectively convert fixed CO<sub>2</sub> to CH<sub>4</sub> under light conditions  
540 appears intricately linked to the photosynthetic process (Bižić et al., 2020; Klintzsch et al., 2020) as inhibitors of photosynthesis  
541 blocked CH<sub>4</sub> production under light conditions (Bižić et al., 2020). They suggest that distinct mechanisms might govern CH<sub>4</sub>  
542 production under light and dark conditions, influenced by freshly synthesized photosynthetic products in light and storage  
543 compounds during darkness.

544 During Phase I, temporal CH<sub>4</sub> accumulation consistently demonstrates higher CH<sub>4</sub> levels in the CC treatment compared to the  
545 NC and <3 μm fraction (controls) (Fig. 7A). However, a noteworthy contrast appears when considering the impact of substrate  
546 additions. Specifically, the introduction of TMA in the CC treatment in this phase results in a more pronounced CH<sub>4</sub> production  
547 (Fig. 7C) compared to the effect of MPn (Fig. 7B). This pattern, the opposite of that found in Phase II, could potentially be  
548 explained by the observed decrease in *Synechococcus* abundance (Fig. S5D), which remains unresponsive to MPn, and the  
549 concurrent increase in nano and picoeukaryotes and bacteria at the end of the experiment (Fig. S5E and F); the last of which  
550 is conducive to the action of TMA (Bižić-Ionescu et al., 2018; De Angelis and Lee, 1994; Lidbury et al., 2015). Indeed, a  
551 marked reduction in *Synechococcus* abundance is observed (showing a 4.6-fold decrease) compared to the Phase II (Fig. S5A  
552 and D), whereas nano- and picoeukaryotes experience notable abundance (3.1 to 3.7 times higher than the transition period)  
553 (Fig. S5B and E).

554



555

556

557

558

559

**Figure 7. Time courses of dissolved methane (nM) during incubation in long-term microcosm experiments (10L) with the addition of methylated substrates (MPn: methyl phosphonic acid and TMA: trimethylamine) performed with three planktonic communities (NC: natural community; <3 μm: bacterioplankton and CC: community concentrate) under oxygenated conditions in September 2019. Photoperiod is represented in white (light) and gray (dark).**

560

561

562

563

564

565

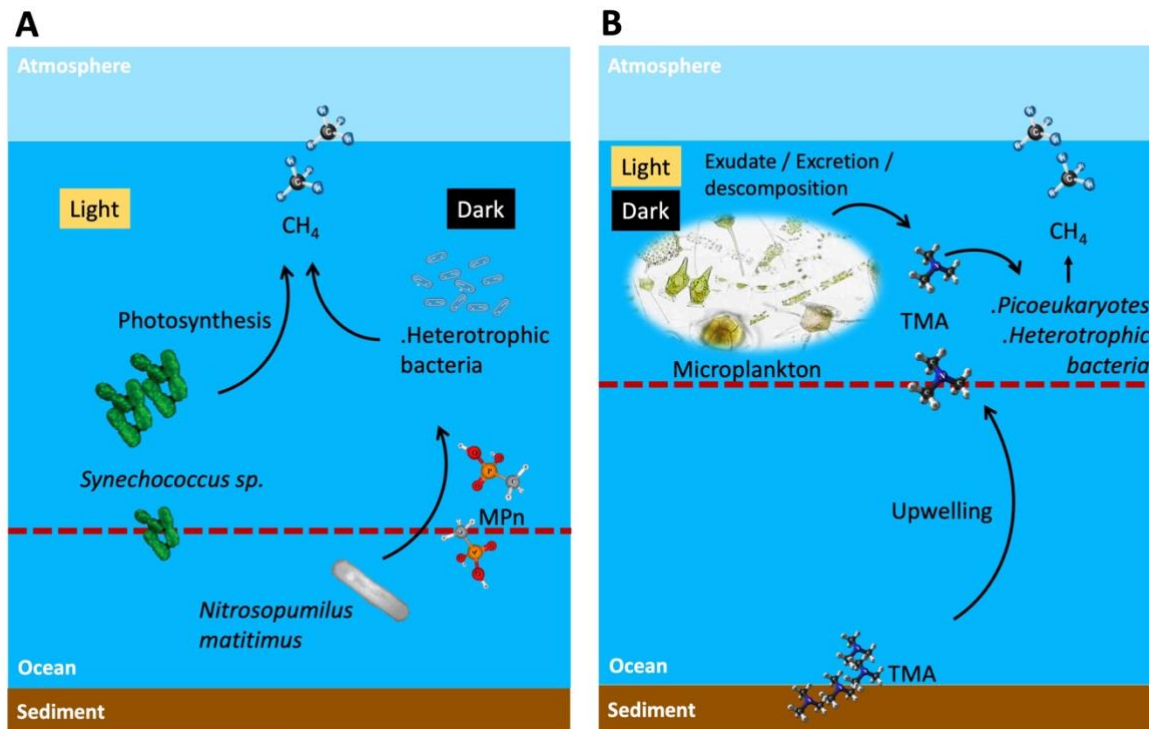
566

567

568

569

In this phase (I), the distribution proportions within the NC treatment are cyanobacteria, nano and picoeukaryotes, and bacteria accounted for 1.1, 2.3 and 96.6, respectively. In contrast, within the CC treatment, the initial distribution proportions are higher with respect to the NC: cyanobacteria, picoeukaryotes, and bacterioplankton displayed proportions 1.6, 0.6, and 2.9 times greater, respectively. This underscores the increased significance of bacteria and autotrophic picoeukaryotes during this phase, as further corroborated by Chl-a measurements (Table S3). An intricate interplay between microbial communities and CH<sub>4</sub> cycling within distinct phases of productivity is schematically illustrate in Figure 8. The prevalence of cyanobacteria, picoeukaryotes, and heterotrophic bacteria varied significantly between these phases. So, this indicates that substrate utilization is related to the availability of nutrients as well as the complexity of the substrate and the composition of the heterotrophic bacterial community, potentially driving CH<sub>4</sub> production dynamics.



570

571

572

573

574

575

Figure 8. Suggested scheme of methane cycling mechanisms in two contrasting periods of primary production and oceanographic conditions during light and dark phases, where potential planktonic communities and methylated substrates are involved to metabolize methane in surface waters. A. Phase II and III or late upwelling or non-upwelling season and B. Phase I or active upwelling season. Dashed line shows the  $100 \mu\text{mol L}^{-1}$  oxycline, above this line oxic methane is produced. TMA: trimethylamine; and MPn: methyl phosphonic acid.

576

577

578

579

580

581

High  $\text{CH}_4$  levels in surface water during the non-upwelling period, comparable to the upwelling period, could result from in situ  $\text{CH}_4$  production mediated by photosynthetic *Synechococcus* or demethylation by heterotrophic bacteria (Fig. 8A). On the other hand, although the trimethylamine methyltransferase enzyme has been described as involved in the demethylation of TMA in methanogen microorganisms (Paul et al., 2000), it cannot be ruled out that in Phase I (spring) heterotrophic bacteria dominance can metabolize TMA through an alternative pathway still unknown (Fig. 8B), nor can it be ruled out that the upwelling brings methanogens with the necessary machinery to metabolize TMA at the ocean surface.

582

#### 4 Conclusions

583

584

585

586

Overall, picoplankton produced  $\text{CH}_4$  in all experiments conducted in both light and dark conditions, although the net  $\text{CH}_4$  production rate was higher in dark conditions. Moreover, laboratory experiments demonstrated that organic compounds such as TMA and MPn are metabolized by heterotrophic bacterioplankton, contributing to the production of oxic  $\text{CH}_4$  in the oxygenated surface layer.



587 Coastal upwelling could bring with it organic amino compounds such as TMA including mono and di trimethylamines from  
588 sediments, which added to plankton decomposition compounds, and change in picoplanktonic composition (bacteria and the  
589 remarkable increase of pico- and nano eukaryotes) during the favorable upwelling period, could promote CH<sub>4</sub> production via  
590 TMA, through a pathway that is still unknown, but would potentially add to CH<sub>4</sub> supersaturation in the oxygenated surface  
591 layer, beyond the contribution of CH<sub>4</sub> by advection.

592 *Synechococcus* could be responsible for CH<sub>4</sub> regeneration through photosynthesis. These cyanobacteria are abundant in the  
593 non-upwelling period, and together with other picoeukaryotes, maintain intermediate and basal Chl-a levels during this period  
594 that matched with higher DOC levels and inorganic N:P ratios (compared to the upwelling period). This may stimulate  
595 heterotrophic bacteria to metabolize MPn and thus contribute to the recycling of oxic CH<sub>4</sub>.

596 It is important to note that amended experiments were conducted in Phase II (March 2019) and Phase III (May 2019), periods  
597 marked by changes in the phytoplankton succession (composition), biomass and abundance in winter, the relative abundance  
598 of picoplankton with respect to microplankton (particularly the presence of *Synechococcus* and *nitrifying archaea*) increases  
599 significantly, especially photosynthetic picoeukaryotes

600 **Acknowledgements** Thanks to Gerardo Garcia for his experience and teaching in the use of laboratory equipment and his help  
601 in setting up the experiments; and Karen Sanzana for nutrient analysis; Oliver Alarcon for oxygen analysis. Both the crew of  
602 R/V Kay Kay (II) and the Dichato Marine Station of the University of Concepcion provided valuable help during fieldwork,  
603 as well as all participating colleagues in the time series station (University of Concepcion), who provided the core  
604 measurements. We also appreciate the work done during the COVID pandemic by Juan Faúndez. This research was funded  
605 by the Fondo Nacional de Investigaciones Científicas y Tecnológicas (FONDECYT) grant N° 1200861 and also  
606 Millennium Science Initiative Program ICM 2019-015 (SECOS) and CR2 FONDAP-CONICYT N° 1522A001.

607

608 **References**

- 609 Aguirre, C., Pizarro, Ó., Strub, P. T., Garreaud, R., and Barth, J. A.: Seasonal dynamics of the near-surface alongshore flow  
610 off central Chile, *J Geophys Res Oceans*, 117, <https://doi.org/10.1029/2011JC007379>, 2012.
- 611 Aguirre, C., Garreaud, R., Belmar, L., Farías, L., Ramajo, L., and Barrera, F.: High-frequency variability of the surface ocean  
612 properties off central Chile during the upwelling season, *Front Mar Sci*, 8, 1–19, <https://doi.org/10.3389/fmars.2021.702051>,  
613 2021.
- 614 Aldunate, M., De la Iglesia, R., Bertagnolli, A. D., and Ulloa, O.: Oxygen modulates bacterial community composition in the  
615 coastal upwelling waters off central Chile, *Deep Sea Research Part II Topical Studies in Oceanography*, 156, 68–79,  
616 <https://doi.org/10.1016/j.dsr2.2018.02.001>, 2018.
- 617 Allen, L. Z., Allen, E. E., Badger, J. H., McCrow, J. P., Paulsen, I. T., Elbourne, L. D., Thiagarajan, M., Rusch, D. B., Neelson,  
618 K. H., Williamson, S. J., Venter, J. C., and Allen, A. E.: Influence of nutrients and currents on the genomic composition of  
619 microbes across an upwelling mosaic, *ISME Journal*, 6, 1403–1414, <https://doi.org/10.1038/ismej.2011.201>, 2012.
- 620 Anabalón, V., Morales, C. E., Escribano, R., Varas, A. M., and Varas, M. A.: The contribution of nano- and micro-planktonic  
621 assemblages in the surface layer (0-30 m) under different hydrographic conditions in the upwelling area off Concepción,  
622 central Chile, *Prog Oceanogr*, 75, 396–414, <https://doi.org/10.1016/j.pocean.2007.08.023>, 2007.
- 623 De Angelis, M. A. and Lee, C.: Methane production during zooplankton grazing on marine phytoplankton, *Limnol. Oceanogr.*,  
624 39, 1298–1308, 1994.
- 625 Bange, H. W., Bartell, U. H., Rapsomanikis, S., and Andreae, M. O.: Methane in the Baltic and North Seas and a reassessment  
626 of the marine emissions of methane, *Global Biogeochem Cycles*, 8, 465–480, 1994.
- 627 Bauer, J. and Druffel, E.: Ocean margins as a significant source of organic matter to the deep open ocean, *Letter to nature*,  
628 392, 482–485, <https://doi.org/10.1038/33122>, 1998.
- 629 Bello, E.: Variabilidad estacional en la descarga de metano disuelto desde un sistema estuarino a la zona marina adyacente, el  
630 caso de ríos de la zona central de Chile (río Itata), Universidad de Concepción, 76 pp., 2016.
- 631 Belviso, S., Kim, S. -K., Rassoulzadegan, F., Krajka, B., Nguyen, B. C., Mihalopoulos, N., and Buat-Menard, P.: Production  
632 of dimethylsulfonium propionate (DMSP) and dimethylsulfide (DMS) by a microbial food web, *Limnol Oceanogr*, 35, 1810–  
633 1821, <https://doi.org/10.4319/lo.1990.35.8.1810>, 1990.
- 634 Benner, R., Dean Pakulski, J., McCarthy, M., Hedges, J. I., Hatcher, P. G., Benner, R., Pakulski, J. D., McCarthy, M., Hedges,  
635 J. I., Hatcher, P. G., H van Beest, B. W., Kramer, G. J., and van Santen, R. A.: Bulk chemical characteristics of dissolved  
636 organic matter in the ocean, *J. Glinnemann, ibid*, 255, 1561–1564, [https://doi.org/DOI: 10.1126/science.255.5051.1561](https://doi.org/DOI:10.1126/science.255.5051.1561), 1992.
- 637 Berg, A., Lindblad, P., and Svensson, B. H.: Cyanobacteria as a source of hydrogen for methane formation, *World J Microbiol*  
638 *Biotechnol*, 30, 539–545, <https://doi.org/10.1007/s11274-013-1463-5>, 2014.
- 639 Bianchi, T. S.: The role of terrestrially derived organic carbon in the coastal ocean: A changing paradigm and the priming  
640 effect, <https://doi.org/10.1073/pnas.1017982108>, 6 December 2011.

641 Bizic, M.: Phytoplankton photosynthesis: An unexplored source of biogenic methane emission from oxic environments, *J*  
642 *Plankton Res*, 43, 822–830, <https://doi.org/10.1093/plankt/fbab069>, 2021.

643 Bižić, M., Klintzsch, T., Ionescu, D., Hindiyeh, M. Y., Günthel, M., Muro-Pastor, A. M., Eckert, W., Urich, T., Keppler, F.,  
644 and Grossart, H. P.: Aquatic and terrestrial cyanobacteria produce methane, *Sci Adv*, 6, 1–10,  
645 <https://doi.org/10.1126/sciadv.aax5343>, 2020.

646 Bižić-Ionescu, M., Ionescu, D., Günthel, M., Tang, K. W., and Grossart, H. P.: Oxic methane cycling: new evidence for  
647 methane formation in oxic lake water, *Biogenesis of Hydrocarbons*, 1–22, <https://doi.org/10.1007/978-3-319-53114-4>, 2018.

648 Borges, A. V. and Abril, G.: Carbon Dioxide and Methane Dynamics in Estuaries, Elsevier Inc., 119–161 pp.,  
649 <https://doi.org/10.1016/B978-0-12-374711-2.00504-0>, 2012.

650 Broecker, W. S. and Peng, T. H.: Gas exchange rates between air and sea, *Tellus XXVI*, 1, 21–35,  
651 <https://doi.org/10.1111/j.2153-3490.1974.tb01640.x>, 1974.

652 Broman, E., Barua, R., Donald, D., Roth, F., Humborg, C., Norkko, A., Jilbert, T., Bonaglia, S., and Nascimento, F. J. A.: No  
653 evidence of light inhibition on aerobic methanotrophs in coastal sediments using eDNA and eRNA, *Environmental DNA*, 5,  
654 766–781, <https://doi.org/10.1002/edn3.441>, 2023.

655 Brown, I. J., Torres, R., and Rees, A. P.: The origin of sub-surface source waters define the sea-air flux of methane in the  
656 Mauritanian Upwelling, NW Africa, *Dynamics of Atmospheres and Oceans*, 67, 39–46,  
657 <https://doi.org/10.1016/j.dynatmoce.2014.06.001>, 2014.

658 Bullister, J. L., Wisegarver, D. P., and Wilson, S. T.: The production of methane and nitrous oxide gas standards for Scientific  
659 Committee on Ocean Research (SCOR) Working Group #143, 1–9 pp., 2016.

660 Capelle, D. W. and Tortell, P. D.: Factors controlling methane and nitrous-oxide variability in the southern British Columbia  
661 coastal upwelling system, *Mar Chem*, 179, 56–67, <https://doi.org/10.1016/j.marchem.2016.01.011>, 2016.

662 Capone, D. G. and Hutchins, D. A.: Microbial biogeochemistry of coastal upwelling regimes in a changing ocean,  
663 <https://doi.org/10.1038/ngeo1916>, September 2013.

664 Carini, P., White, A. E., Campbell, E. O., and Giovannoni, S. J.: Methane production by phosphate-starved SAR11  
665 chemoheterotrophic marine bacteria, *Nat Commun*, 5, 1–7, <https://doi.org/10.1038/ncomms5346>, 2014.

666 Carpenter, J.: Do rats and pigeons readily acquire instrumental responses for food in the presence of free food?, *Limnol*  
667 *Oceanogr*, 10, 141–143, <https://doi.org/10.3758/BF03209628>, 1965.

668 Carpenter, L. J., Archer, S. D., and Beale, R.: Ocean-atmosphere trace gas exchange, *Chem Soc Rev*, 41, 6473–6506,  
669 <https://doi.org/10.1039/c2cs35121h>, 2012.

670 Cerbin, S., Pérez, G., Rybak, M., Wejnerowski, Ł., Konowalczyk, A., Helmsing, N., Naus-Wiezer, S., Meima-Franke, M.,  
671 Pytlak, Ł., Raaijmakers, C., Nowak, W., and Bodelier, P. L. E.: Methane-derived carbon as a driver for cyanobacterial growth,  
672 *Front Microbiol*, 13, 1–16, <https://doi.org/10.3389/fmicb.2022.837198>, 2022.

673 Cicerone, R. J. and Oremland, R. S.: Biogeochemical aspects of atmospheric methane, *Global Biogeochem Cycles*, 2, 299–  
674 327, <https://doi.org/10.1029/GB002i004p00299>, 1988.

675 Collado-Fabbri, S., Vaultot, D., and Ulloa, O.: Structure and seasonal dynamics of the eukaryotic picophytoplankton  
676 community in a wind-driven coastal upwelling ecosystem, *Limnol. Oceanogr.*, 56, 2334–2346,  
677 <https://doi.org/10.4319/lo.2011.56.6.2334>, 2011.

678 Cuevas, L. A., Daneri, G., Jacob, B., and Montero, P.: Microbial abundance and activity in the seasonal upwelling area off  
679 Concepción (~36°S), central Chile: A comparison of upwelling and non-upwelling conditions, *Deep Sea Res 2 Top Stud*  
680 *Oceanogr.*, 51, 2427–2440, <https://doi.org/10.1016/j.dsr2.2004.07.026>, 2004.

681 Damm, E., Helmke, E., Thoms, S., Schauer, U., Nöthing, E., Bakker, K., and Kiene, R. P.: Methane production in aerobic  
682 oligotrophic surface water in the central Arctic Ocean, *Biogeosciences*, 7, 1099–1108, [https://doi.org/10.5194/bgd-6-10355-](https://doi.org/10.5194/bgd-6-10355-2009)  
683 2009, 2010.

684 Damm, E., Beszczynska-Möller, T. A., Nöthing, E. M., and Kattner, G.: Methane excess production in oxygen-rich polar water  
685 and a model of cellular conditions for this paradox, *Polar Sci*, 9, 327–334, <https://doi.org/10.1016/j.polar.2015.05.001>, 2015.

686 Dinasquet, J., Tirola, M., and Azam, F.: Enrichment of bacterioplankton able to utilize one-carbon and methylated compounds  
687 in the Coastal Pacific Ocean, *Front Mar Sci*, 5, 1–13, <https://doi.org/10.3389/fmars.2018.00307>, 2018.

688 Dumestre, J. F., Guézennec, J., Galy-Lacaux, C., Delmas, R., Richard, S., and Labroue, L.: Influence of light intensity on  
689 methanotrophic bacterial activity in Petit Saut Reservoir, French Guiana, *Appl Environ Microbiol*, 65, 534–539,  
690 <https://doi.org/10.1128/aem.65.2.534-539.1999>, 1999.

691 Farías, L., Graco, M., and Ulloa, O.: Temporal variability of nitrogen cycling in continental-shelf sediments of the upwelling  
692 ecosystem off central Chile, *Deep Sea Res 2 Top Stud Oceanogr.*, 51, 2491–2505, <https://doi.org/10.1016/j.dsr2.2004.07.029>,  
693 2004.

694 Farías, L., Fernández, C., Faúndez, J., Cornejo, M., and Alcaman, M. E.: Chemolithoautotrophic production mediating the  
695 cycling of the greenhouse gases N<sub>2</sub>O and CH<sub>4</sub> in an upwelling ecosystem, *Biogeosciences*, 6, 3053–3069,  
696 <https://doi.org/https://doi.org/10.5194/bg-6-3053-2009>, 2009.

697 Farías, L., Besoain, V., and García-Loyola, S.: Presence of nitrous oxide hotspots in the coastal upwelling area off central  
698 Chile: an analysis of temporal variability based on ten years of a biogeochemical time series, *Environmental Research Letters*,  
699 10, 1–13, <https://doi.org/10.1088/1748-9326/10/4/044017>, 2015.

700 Farías, L., Tenorio, S., Sanzana, K., and Faundez, J.: Temporal methane variability in the water column of an area of seasonal  
701 coastal upwelling: A study based on a 12 year time series, *Prog Oceanogr.*, 195, <https://doi.org/10.1016/j.pocean.2021.102589>,  
702 2021.

703 Ferderlman, T. G., Lee, C., Pantoja, S., Harder, J., Bebout, B. M., and Fossing, H.: Sulfate reduction and methanogenesis in a  
704 Thioploca- dominates sediment off the coast of Chile, *Geochim Cosmochim Acta*, 61, 3065–3079,  
705 [https://doi.org/https://doi.org/10.1016/S0016-7037\(97\)00158-0](https://doi.org/https://doi.org/10.1016/S0016-7037(97)00158-0), 1997.

706 Fernandez, C., González, M. L., Muñoz, C., Molina, V., and Farias, L.: Temporal and spatial variability of biological nitrogen  
707 fixation off the upwelling system of central Chile (35–38.5°S), *J Geophys Res Oceans*, 120, 3330–3349,  
708 <https://doi.org/10.1002/2014JC010410>, 2015.

709 Florez-Leiva, L., Damm, E., Farías, L., and Fariás, L.: Methane production induced by dimethylsulfide in surface water of an  
710 upwelling ecosystem, *Prog Oceanogr*, 112–113, 38–48, <https://doi.org/10.1016/j.pocean.2013.03.005>, 2013.

711 Gibb, S. W., Mantoura, R. F. C., Liss, P. S., and Barlow, R. G.: Distributions and biogeochemistries of methylamines and  
712 ammonium in the Arabian Sea, *Deep Sea Res 2 Top Stud Oceanogr*, 46, 593–615, [https://doi.org/10.1016/S0967-](https://doi.org/10.1016/S0967-0645(98)00119-2)  
713 [0645\(98\)00119-2](https://doi.org/10.1016/S0967-0645(98)00119-2), 1999.

714 Giovannoni, S. J., Delong, E. F., Schmidt, T. M., and Pace, N. R.: Tangential flow filtration and preliminary phylogenetic  
715 analysis of marine picoplankton, *Appl Environ Microbiol*, 56, 2572–2575, 1990.

716 González, H. E., Menschel, E., Aparicio, C., and Barría, C.: Spatial and temporal variability of microplankton and detritus,  
717 and their export to the shelf sediments in the upwelling area off Concepción, Chile (~36°S), during 2002-2005, *Prog Oceanogr*,  
718 75, 435–451, <https://doi.org/10.1016/j.pocean.2007.08.025>, 2007.

719 Grasshoff, K., Ehrhardt, M., and Kremling, K.: *Methods of Seawater Analysis*. Second, Second, Re., John Wiley & Sons, Ltd,  
720 Deerfield Beach, Florida: Verlag Chemie, 419 pp., <https://doi.org/10.1002/iroh.19850700232>, 1983.

721 Grossart, H. P., Frindte, K., Dziallas, C., Eckert, W., and Tang, K. W.: Microbial methane production in oxygenated water  
722 column of an oligotrophic lake, *Proc Natl Acad Sci U S A*, 108, 19657–19661, <https://doi.org/10.1073/pnas.1110716108>,  
723 2011.

724 Günthel, M., Donis, D., Kirillin, G., Ionescu, D., Bizic, M., McGinnis, D. F., Grossart, H. P., and Tang, K. W.: Contribution  
725 of oxic methane production to surface methane emission in lakes and its global importance, *Nat Commun*, 10,  
726 <https://doi.org/10.1038/s41467-019-13320-0>, 2019.

727 Günthel, M., Klawonn, I., Woodhouse, J., Bižić, M., Ionescu, D., Ganzert, L., Kümmel, S., Nijenhuis, I., Zoccarato, L.,  
728 Grossart, H. P., and Tang, K. W.: Photosynthesis-driven methane production in oxic lake water as an important contributor to  
729 methane emission, *Limnol Oceanogr*, 1–13, <https://doi.org/10.1002/lno.11557>, 2020.

730 Hahn, M. W.: Broad diversity of viable bacteria in “sterile” (0.2 µm) filtered water, *Res Microbiol*, 155, 688–691,  
731 <https://doi.org/10.1016/j.resmic.2004.05.003>, 2004.

732 Hansell, D. A. and Orellana, M. V.: *Dissolved organic matter in the global ocean: A primer*,  
733 <https://doi.org/10.3390/gels7030128>, 1 September 2021.

734 Harmsen, M., van Vuuren, D. P., Bodirsky, B. L., Chateau, J., Durand-Lasserre, O., Drouet, L., Fricko, O., Fujimori, S.,  
735 Gernaat, D. E. H. J., Hanaoka, T., Hilaire, J., Keramidis, K., Luderer, G., Moura, M. C. P., Sano, F., Smith, S. J., and Wada,  
736 K.: The role of methane in future climate strategies: mitigation potentials and climate impacts, *Clim Change*, 163, 1409–1425,  
737 <https://doi.org/10.1007/s10584-019-02437-2>, 2020.

738 Hartmann, J. F., Günthel, M., Klintzsch, T., Kirillin, G., Grossart, H. P., Keppler, F., and Isenbeck-Schröter, M.: High  
739 spatiotemporal dynamics of methane production and emission in oxic surface water, *Environ Sci Technol*, 54, 1451–1463,  
740 <https://doi.org/10.1021/acs.est.9b03182>, 2020.

741 Holmes, E. M., Sansone, F. J., Rust, T. M., and Popp, B. N.: Methane production, consumption, and air-sea exchange in the  
742 open ocean: An evaluation based on carbon isotopic ratios, *Global Biogeochem Cycles*, 14, 1–10,  
743 <https://doi.org/10.1029/1999GB001209>, 2000.

744 Holm-Hansen, O., Lorenzen, C. J., Holmes, R. W., and Strickland, J. D. H.: Fluorometric determination of chlorophyll, *Journal*  
745 *du Conseil International pour L’Exploration de la Mer*, 30, 3–15, <https://doi.org/10.1093/icesjms/30.1.3>, 1965.

746 Igarza, M., Dittmar, T., Graco, M., and Niggemann, J.: Dissolved organic matter cycling in the coastal upwelling system off  
747 central Peru during an “El Niño” year, *Front Mar Sci*, 6, 1–17, <https://doi.org/10.3389/fmars.2019.00198>, 2019.

748 IPCC: Climate change 2021: the physical science basis. Working Group I contribution to the IPCC sixth assessment report,  
749 Cambridge University Press, 35–144 pp., 2021.

750 Jacob, B. G., Tapia, F. J., Quiñones, R. A., Montes, R., Sobarzo, M., Schneider, W., Daneri, G., Morales, C. E., Montero, P.,  
751 and González, H. E.: Major changes in diatom abundance, productivity, and net community metabolism in a windier and dryer  
752 coastal climate in the southern Humboldt Current, *Prog Oceanogr*, 168, 196–209,  
753 <https://doi.org/10.1016/j.pocean.2018.10.001>, 2018.

754 Kara, A. B., Rochford, P. A., and Hurlburt, H. E.: Mixed layer depth variability over the global ocean, *J Geophys Res Oceans*,  
755 108, 1–15, <https://doi.org/10.1029/2000jc000736>, 2003.

756 Karl, D. and Tilbrook, B.: Production and transport of methane in oceanic particulate organic matter, *Nature*, 368, 732–734,  
757 1994.

758 Karl, D., Beversdorf, L., Björkman, K., Church, M., Martinez, A., and DeLong, E.: Aerobic production of methane in the sea,  
759 *Nat Geosci*, 1, 473–478, <https://doi.org/10.1038/ngeo234>, 2008.

760 Klintzsch, T., Langer, G., Nehrke, G., Wieland, A., Lenhart, K., and Keppler, F.: Methane production by three widespread  
761 marine phytoplankton species: release rates, precursor compounds, and relevance for the environment, *Biogeosciences*, 16,  
762 4129–4144, <https://doi.org/10.5194/bg-2019-245>, 2019.

763 Klintzsch, T., Langer, G., Wieland, A., Geisinger, H., Lenhart, K., Nehrke, G., and Keppler, F.: Effects of temperature and  
764 light on methane production of widespread marine phytoplankton, *J Geophys Res Biogeosci*, 125, 1–16,  
765 <https://doi.org/10.1029/2020JG005793>, 2020.

766 Klintzsch, T., Geisinger, H., Wieland, A., Langer, G., Nehrke, G., Bizic, M., Greule, M., Lenhart, K., Borsch, C., Schroll, M.,  
767 and Keppler, F.: Stable carbon isotope signature of methane released from phytoplankton, *Geophys Res Lett*, 50, 1–12,  
768 <https://doi.org/10.1029/2023gl1103317>, 2023.

769 Kock, A., Gebhardt, S., and Bange, H. W. W.: Methane emissions from the upwelling area off Mauritania (NW Africa),  
770 *Biogeosciences*, 5, 1119–1125, <https://doi.org/10.5194/bg-5-1119-2008>, 2008.

771 De La Iglesia, R., Echenique-Subiabre, I., Rodríguez-Marconi, S., Espinoza, J. P., Von Dassow, P., Ulloa, O., and Trefault,  
772 N.: Distinct oxygen environments shape picoeukaryote assemblages thriving oxygen minimum zone waters off central Chile,  
773 *J Plankton Res*, 42, 514–529, <https://doi.org/10.1093/plankt/fbaa036>, 2020.

774 Lamontagne, R. A., Swinnerton, J. W., Linnenbom, V. J., and Smith, W. D.: Methane concentrations in various marine  
775 environments, *J Geophys Res*, 78, 5317–5324, <https://doi.org/10.1029/JC078i024p05317>, 1973.

776 Lenhart, K., Klintzsch, T., Langer, G., Nehrke, G., Bunge, M., Schnell, S., and Keppler, F.: Evidence for methane production  
777 by the marine algae *Emiliania huxleyi*, *Biogeosciences*, 13, 3163–3174, <https://doi.org/10.5194/bg-13-3163-2016>, 2016.

778 León-Palmero, E., Contreras-Ruiz, A., Sierra, A., Morales-Baquero, R., and Reche, I.: Dissolved CH<sub>4</sub> coupled to  
779 photosynthetic picoeukaryotes in oxic waters and to cumulative chlorophyll a in anoxic waters of reservoirs, *Biogeosciences*,  
780 17, 1–23, <https://doi.org/10.5194/bg-17-3223-2020>, 2020.

781 Li, Y., Fichot, C. G., Geng, L., Scarratt, M. G., and Xie, H.: The contribution of methane photoproduction to the oceanic  
782 methane paradox, *Geophys Res Lett*, 47, 1–10, <https://doi.org/10.1029/2020GL088362>, 2020.

783 Lidbury, I. D. E. A., Murrell, J. C., and Chen, Y.: Trimethylamine and trimethylamine N-oxide are supplementary energy  
784 sources for a marine heterotrophic bacterium: Implications for marine carbon and nitrogen cycling, *ISME Journal*, 9, 760–769,  
785 <https://doi.org/10.1038/ismej.2014.149>, 2015.

786 Llabrés, M., Agustí, S., and Herndl, G. J.: Diel in situ picophytoplankton cell death cycles coupled with cell division, *J Phycol*,  
787 47, 1247–1257, <https://doi.org/10.1111/j.1529-8817.2011.01072.x>, 2011.

788 Lohrer, C., Cwierz, P. P., Wirth, M. A., Schulz-Bull, D. E., and Kanwischer, M.: Methodological aspects of methylphosphonic  
789 acid analysis: Determination in river and coastal water samples, *Talanta*, 211, 1–8,  
790 <https://doi.org/10.1016/j.talanta.2020.120724>, 2020.

791 Lu, X., Jacob, D. J., Zhang, Y., Maasackers, J. D., Sulprizio, M. P., Shen, L., Qu, Z., Scarpelli, T. R., Nesser, H., Yantosca,  
792 R. M., Sheng, J., Andrews, A., Parker, R. J., Boesch, H., Anthony Bloom, A., and Ma, S.: Global methane budget and trend,  
793 2010-2017: Complementarity of inverse analyses using in situ (globalviewplus ch4 obspack) and satellite (gosat) observations,  
794 <https://doi.org/10.5194/acp-21-4637-2021>, 25 March 2021.

795 Ma, X., Sun, M., Lennartz, S. T., and Bange, H. W.: A decade of methane measurements at the Boknis Eck Time-series Station  
796 in the Eckernförde Bay (Southwestern Baltic Sea), *Biogeosciences Discussions*, 2020, 1–22, <https://doi.org/10.5194/bg-2020-107>, 2020.

798 Mao, S. H., Zhang, H. H., Zhuang, G. C., Li, X. J., Liu, Q., Zhou, Z., Wang, W. L., Li, C. Y., Lu, K. Y., Liu, X. T., Montgomery,  
799 A., Joye, S. B., Zhang, Y. Z., and Yang, G. P.: Aerobic oxidation of methane significantly reduces global diffusive methane  
800 emissions from shallow marine waters, *Nat Commun*, 13, <https://doi.org/10.1038/s41467-022-35082-y>, 2022.

801 Martínez, A., Ventouras, L. A., Wilson, S. T., Karl, D. M., and DeLong, E. F.: Metatranscriptomic and functional metagenomic  
802 analysis of methylphosphonate utilization by marine bacteria, *Front Microbiol*, 4, <https://doi.org/10.3389/fmicb.2013.00340>,  
803 2013.

804 McAuliffe, C.: Solubility in water of C<sub>1</sub>-C<sub>9</sub> hydrocarbons, *Nature*, 200, 1092–1093, 1963.

805 McClain, M. E., Boyer, E. W., Dent, C. L., Gergel, S. E., Grimm, N. B., Groffman, P. M., Hart, S. C., Harvey, J. W., Johnston,  
806 C. A., Mayorga, E., McDowell, W. H., and Pinay, G.: Biogeochemical Hot Spots and Hot Moments at the Interface of  
807 Terrestrial and Aquatic Ecosystems, <https://doi.org/10.1007/s10021-003-0161-9>, June 2003.

808 Metcalf, W. W., Griffin, B. M., Cicchillo, R., Gao, J., Janga, S., Cooke, H., Circello, B., Evans, B., Martens-Habbena, W.,  
809 Stahl, D., and Van Der Donk, W.: Synthesis of methylphosphonic acid by marine microbes: a source for methane in the  
810 Aerobic Ocean, *Science* (1979), 337, 1104–1107, <https://doi.org/10.1126/science.1219875>, 2012.

811 Minor, E. C., Swenson, M. M., Mattson, B. M., and Oyler, A. R.: Structural characterization of dissolved organic matter: A  
812 review of current techniques for isolation and analysis, *Environmental Sciences: Processes and Impacts*, 16, 2064–2079,  
813 <https://doi.org/10.1039/c4em00062e>, 2014.

814 Molina, V., Belmar, L., Levipan, H. A., Ramírez-Flandes, S., Anguita, C., Galán, A., Montes, I., and Ulloa, O.: Spatiotemporal  
815 distribution of key pelagic microbes in a seasonal oxygen-deficient coastal upwelling system of the Eastern South Pacific  
816 Ocean, *Front Mar Sci*, 7, 1–17, <https://doi.org/10.3389/fmars.2020.561597>, 2020.

817 Mopper, K., Kieber, D. J., and Stubbins, A.: Marine photochemistry of organic matter: processes and impacts. processes and  
818 impacts., in: *Biogeochemistry of Marine Dissolved Organic Matter: Second Edition*, Elsevier Inc., 389–450,  
819 <https://doi.org/10.1016/B978-0-12-405940-5.00008-X>, 2015.

820 Morales, C. and Anabalón, V.: Phytoplankton biomass and microbial abundances during the spring upwelling season in the  
821 coastal area off Concepción , central-southern Chile : variability around a time series station, *Prog Oceanogr*, 92–95, 81–91,  
822 <https://doi.org/10.1016/j.pocean.2011.07.004>, 2012.

823 Morales, C., González, H. E., Hormazabal, S. E., Yuras, G., Letelier, J., and Castro, L. R.: The distribution of chlorophyll- a  
824 and dominant planktonic components in the coastal transition zone off Concepción, central Chile, during different  
825 oceanographic conditions, *Prog Oceanogr*, 75, 452–469, <https://doi.org/10.1016/j.pocean.2007.08.026>, 2007.

826 Morán, X. A. G., Estrada, M., Gasol, J. M., and Pedrós-Alió, C.: Dissolved primary production and the strength of  
827 phytoplankton-bacterioplankton coupling in contrasting marine regions, *Microb Ecol*, 44, 217–223,  
828 <https://doi.org/10.1007/s00248-002-1026-z>, 2002.

829 Morana, C., Bouillon, S., Nolla-Ardèvol, V., Roland, F., Okello, W., Descy, J.-P., Nankabirwa, A., Nabafu, E., Springael, D.,  
830 and Borges, A.: Methane paradox in tropical lakes? Sedimentary fluxes rather than water column production in oxic waters  
831 sustain methanotrophy and emissions to the atmosphere, *Biogeosciences Discussions*, 17, 1–20, [https://doi.org/10.5194/bg-](https://doi.org/10.5194/bg-2020-142)  
832 2020-142, 2020.

833 Muñoz-Marín, M. C., Gómez-Baena, G., López-Lozano, A., Moreno-Cabezuelo, J. A., Díez, J., and García-Fernández, J. M.:  
834 Mixotrophy in marine picocyanobacteria: use of organic compounds by *Prochlorococcus* and *Synechococcus*,  
835 <https://doi.org/10.1038/s41396-020-0603-9>, 1 May 2020.

836 Oremland, R. S.: Methanogenic activity in plankton samples and fish intestines: A mechanism for in situ methanogenesis in  
837 oceanic surface waters, *Limnol. Oceanogr.*, 24, 1136–1141, 1979.

838 Paul, L., Ferguson, D. J., and Krzycki, J. A.: The trimethylamine methyltransferase gene and multiple dimethylamine  
839 methyltransferase genes of *methanosarcina barkeri* contain in-frame and read-through amber codons, *J Bacteriol*, 182, 2520–  
840 2529, [https://doi.org/0021-9193/00/\\$04.00](https://doi.org/0021-9193/00/$04.00)≤0, 2000.



841 Rain-Franco, A., Sobarzo, M., Caparros, J., and Fernandez, C.: Variability of chromophoric dissolved organic matter in three  
842 freshwater-influenced systems along central-southern Chile, *Prog Oceanogr*, 174, 154–161,  
843 <https://doi.org/10.1016/j.pocean.2018.09.009>, 2019.

844 Raven, J. A.: The twelfth tansley lecture. Small is beautiful: the picophytoplankton, *Funct Ecol*, 12, 503–513,  
845 <https://doi.org/10.1046/j.1365-2435.1998.00233.x>, 1998.

846 Reeburgh, W. S.: Oceanic methane biogeochemistry, American Chemical Society, 107, 486–513,  
847 <https://doi.org/10.1021/cr050362v>, 2007.

848 Reintjes, G., Fuchs, B. M., Scharfe, M., Wiltshire, K. H., Amann, R., and Arnosti, C.: Short-term changes in polysaccharide  
849 utilization mechanisms of marine bacterioplankton during a spring phytoplankton bloom, *Environ Microbiol*, 22, 1884–1900,  
850 <https://doi.org/10.1111/1462-2920.14971>, 2020.

851 Repeta, D. J., Ferrón, S., Sosa, O. A., Johnson, C. G., Repeta, L. D., Acker, M., DeLong, E. F., and Karl, D. M.: Marine  
852 methane paradox explained by bacterial degradation of dissolved organic matter, *Nat Geosci*, 9, 1–7,  
853 <https://doi.org/10.1038/ngeo2837>, 2016.

854 Roth, F., Sun, X., Geibel, M. C., Prytherch, J., Brüchert, V., Bonaglia, S., Broman, E., Nascimento, F., Norkko, A., and  
855 Humborg, C.: High spatiotemporal variability of methane concentrations challenges estimates of emissions across vegetated  
856 coastal ecosystems, *Glob Chang Biol*, <https://doi.org/10.1111/gcb.16177>, 2022.

857 Saunio, M., Stavert, A. R., Poulter, B., Bousquet, P., Canadell, J. G., Jackson, R. B., Raymond, P. A., Dlugokencky, E. J.,  
858 and Houweling, S.: The global methane budget 2000 – 2017, *Earth Syst Sci Data*, 12, 1561–1623, [https://doi.org/10.5194/essd-](https://doi.org/10.5194/essd-12-1561-2020)  
859 [12-1561-2020](https://doi.org/10.5194/essd-12-1561-2020), 2020.

860 Schlitzer, R.: Ocean Data View, 2023.

861 Sieburth, J., Smetacek, V., and Lenz, J.: Pelagic ecosystem structure: Heterotrophic compartments of the plankton and their  
862 relationship to plankton size fractions, *Limnol. Oceanogr.*, 23, 1256–1263, <https://doi.org/10.4319/lo.1978.23.6.1256>, 1978.

863 Smith, M. W., Allen, L. Z., Allen, A. E., Herfort, L., and Simon, H. M.: Contrasting genomic properties of free-living and  
864 particle-attached microbial assemblages within a coastal ecosystem, *Front Microbiol*, 4, 1–20,  
865 <https://doi.org/10.3389/fmicb.2013.00120>, 2013.

866 Sobarzo, M. and Djurfeldt, L.: Coastal upwelling process on a continental shelf limited by submarine canyons, Concepción,  
867 central Chile, *J Geophys Res*, 109, 1–20, <https://doi.org/10.1029/2004JC002350>, 2004.

868 Sobarzo, M., Bravo, L., Donoso, D., Garcés-Vargas, J., and Schneider, W.: Coastal upwelling and seasonal cycles that  
869 influence the water column over the continental shelf off central Chile, *Prog Oceanogr*, 75, 363–382,  
870 <https://doi.org/10.1016/j.pocean.2007.08.022>, 2007.

871 Sosa, O. A., Repeta, D. J., DeLong, E. F., Ashkezari, M. D., and Karl, D. M.: Phosphate-limited ocean regions select for  
872 bacterial populations enriched in the carbon–phosphorus lyase pathway for phosphonate degradation, *Environ Microbiol*, 21,  
873 2402–2414, <https://doi.org/10.1111/1462-2920.14628>, 2019.

874 Sosa, O. A., Burrell, T. J., Wilson, S. T., Foreman, R. K., Karl, D. M., and Repeta, D. J.: Phosphonate cycling supports methane  
875 and ethylene supersaturation in the phosphate-depleted western North Atlantic Ocean, *Limnol Oceanogr*, 1–17,  
876 <https://doi.org/10.1002/lno.11463>, 2020.

877 Spilling, K., Camarena-Gómez, M. T., Lipssewars, T., Martínez-Varela, A., Díaz-Rosas, F., Eronen-Rasimus, E., Silva, N., von  
878 Dassow, P., and Montecino, V.: Impacts of reduced inorganic N:P ratio on three distinct plankton communities in the Humboldt  
879 upwelling system, *Mar Biol*, 166, 1–17, <https://doi.org/10.1007/s00227-019-3561-x>, 2019.

880 Stefels, J. and Van Boekel, W.: Production of DMS from dissolved DMSP in axenic cultures of the marine phytoplankton  
881 species *Phaeocystis* sp, *Mar Ecol Prog Ser*, 97, 11–18, <https://doi.org/https://www.jstor.org/stable/24833593>, 1993.

882 Strub, T., Mesías, J., Montecino, V., Rutllant, J., and Salinas, S.: Coastal ocean circulation off western south america, in: *The*  
883 *global coastal ocean - regional studies and syntheses*, vol. 11, 273–313, 1998.

884 Sun, J., Steindler, L., Thrash, J. C., Halsey, K. H., Smith, D. P., Carter, A. E., Landry, Z. C., and Giovannoni, S. J.: One carbon  
885 metabolism in SAR11 pelagic marine bacteria, *PLoS One*, 6, 1–12, <https://doi.org/10.1371/journal.pone.0023973>, 2011.

886 Sun, J., Mausz, M. A., Chen, Y., and Giovannoni, S. J.: Microbial trimethylamine metabolism in marine environments, *Environ*  
887 *Microbiol*, 21, 513–520, <https://doi.org/10.1111/1462-2920.14461>, 2019.

888 Taenzer, L.: *The isotope biogeochemistry of methane produced from the C-P lyase pathway*, Dartmouth College, 2019.

889 Testa, G., Masotti, I., and Farías, L.: Temporal variability in net primary production in an upwelling area off central Chile  
890 (36°S), *Front Mar Sci*, 5, 1–17, <https://doi.org/10.3389/fmars.2018.00179>, 2018.

891 Upstill-goddard, R. C. and Barnes, J.: Methane emissions from UK estuaries: Re-evaluating the estuarine source of  
892 tropospheric methane from Europe, 180, 14–23, <https://doi.org/10.1016/j.marchem.2016.01.010>, 2016.

893 Urata, S., Kurosawa, Y., Yamasaki, N., Yamamoto, H., Nishiwaki, N., Hongo, Y., Adachi, M., and Yamaguchi, H.: Utilization  
894 of phosphonic acid compounds by marine bacteria of the genera *Phaeobacter*, *Ruegeria*, and *Thalassospira* ( $\alpha$ -Proteobacteria),  
895 *FEMS Microbiol Lett*, 369, <https://doi.org/10.1093/femsle/fnac065>, 2022.

896 Del Valle, D. A. and Karl, D. M.: Aerobic production of methane from dissolved water-column methylphosphonate and sinking  
897 particles in the North Pacific Subtropical Gyre, *Aquatic Microbial Ecology*, 73, 93–105, <https://doi.org/10.3354/ame01714>,  
898 2014.

899 Vargas, C. A., Martínez, R. A., Cuevas, L. A., Pavez, M. A., Cartes, C., González, H. E., Escribano, R., and Daneri, G.: The  
900 relative importance of microbial and classical food webs in a highly productive coastal upwelling area, *Limnol Oceanogr*, 52,  
901 1495–1510, <https://doi.org/10.4319/lo.2007.52.4.1495>, 2007.

902 Vargas, C. A., Arriagada, L., Sobarzo, M., Contreras, P. Y., and Saldías, G.: Bacterial production along a river-to-ocean  
903 continuum in central Chile: implications for organic matter cycling, *Aquatic Microbial Ecology*, 68, 195–213,  
904 <https://doi.org/10.3354/ame01608>, 2013.

905 Vargas, C. A., Contreras, P. Y., Pérez, C. A., Sobarzo, M., Saldías, G. S., and Salisbury, J.: Influences of riverine and upwelling  
906 waters on the coastal carbonate system off Central Chile and their ocean acidification implications, *J Geophys Res Biogeosci*,  
907 121, 1–16, <https://doi.org/10.1002/2015JG003213>, 2016.

908 Wang, Q., Dore, J. E., and McDermott, T. R.: Methylphosphonate metabolism by *Pseudomonas* sp. populations contributes to  
909 the methane oversaturation paradox in an oxic freshwater lake, *Environ Microbiol*, 19, 1–41, [https://doi.org/10.1111/1462-](https://doi.org/10.1111/1462-2920.13747)  
910 [2920.13747](https://doi.org/10.1111/1462-2920.13747), 2018.

911 Wang, Q., Alowaifeer, A., Kerner, P., Balasubramanian, N., Patterson, A., Christian, W., Tarver, A., Dore, J. E., Hatzepichler,  
912 R., Bothner, B., and McDermott, T. R.: Aerobic bacterial methane synthesis, *Proceedings of the National Academy of*  
913 *Sciences*, 118, 1–9, <https://doi.org/10.1073/pnas.2019229118>, 2021.

914 Wanninkhof, R.: Relationship between wind speed and gas exchange over the ocean, *J Geophys Res*, 97, 7373–7382,  
915 <https://doi.org/10.1029/92JC00188>, 1992.

916 Weber, T., Wiseman, N. A., and Kock, A.: Global ocean methane emissions dominated by shallow coastal waters, *Nat*  
917 *Commun*, 10, 1–10, <https://doi.org/10.1038/s41467-019-12541-7>, 2019.

918 Wiesenburg, D. A. and Guinasso, N. L.: Equilibrium solubilities of methane, carbon monoxide, and hydrogen in water and sea  
919 water, *American Chemical Society*, 24, 356–360, 1979.

920 Worden, A.: Picoeukaryote diversity in coastal waters of the Pacific Ocean, *Aquatic microbial ecology*, 43, 165–175,  
921 <https://doi.org/doi:10.3354/ame043165>, 2006.

922 Xu, S., Sun, Z., Geng, W., Cao, H., Zhang, X., Zhai, B., and Wu, Z.: Advance in Numerical Simulation Research of Marine  
923 Methane Processes, *Front Earth Sci (Lausanne)*, 10, <https://doi.org/10.3389/feart.2022.891393>, 2022.

924 Ye, W. W., Wang, X. L., Zhang, X.-H., and Zhang, G.-L.: Methane production in oxic seawater of the western North Pacific  
925 and its marginal seas, *Limnol Oceanogr*, 65, 1–14, <https://doi.org/10.1002/lno.11457>, 2020.

926 Zhang, Y. and Xie, H.: Photomineralization and photomethanification of dissolved organic matter in Saguenay River surface  
927 water, *Biogeosciences*, 12, 6823–6836, <https://doi.org/10.5194/bg-12-6823-2015>, 2015.

928 Zhao, L., Lin, L.-Z., Chen, M.-Y., Teng, W.-K., Zheng, L.-L., Peng, L., Lv, J., Brand, J. J., Hu, C.-X., Han, B.-P., Song, L.-  
929 R., and Shu, W.-S.: The widespread capability of methylphosphonate utilization in filamentous cyanobacteria and its  
930 ecological significance, *Water Res*, 217, 1–11, <https://doi.org/10.1016/j.watres.2022.118385>, 2022.

931